geosciences

MDPI

Article

Lithium Distribution and Hydrogeochemical Associations in Contrasting Waters of the Mangystau Region, Kazakhstan

Assiya Boranbayeva [1], Raiymbek Sarkulov [2,*], Akmaral Serikbayeva [2,*], Kosarbay Kozhakhmet [2], Azamat Tarbanov [3], Yerbolat Ayapbergenov [3] and Sayat Mameshova [4]

[1] Pedagogy Faculty, Yessenov University, 32 Microdistrict, Aktau 130003, Kazakhstan; assiya.boranbayeva@yu.edu.kz
[2] Engineering Faculty, Yessenov University, 32 Microdistrict, Aktau 130003, Kazakhstan
[3] Branch of Limited Liability Partnership "KazMunaiGas Engineering" "KazNIPImunaigas", 35 Microdistrict, Section 6/1, Aktau 130000, Kazakhstan
[4] Department of Chemistry and Chemical Technology, Taraz University Named After M. H. Dulaty, 13 Suleimenova Street, Taraz 080000, Kazakhstan
* Correspondence: raiymbek2.sarkulov@yu.edu.kz (R.S.); akmaral.serikbayeva@yu.edu.kz (A.S.); Tel.: +7-708-001-62-97 (R.S.); +7-701-515-96-13 (A.S.)

Abstract

Lithium (Li) occurrence in the Mangystau Region of western Kazakhstan has been investigated primarily in deep formation and oilfield brines, whereas surface waters and shallow groundwater remain poorly characterized. This study aimed to establish a regional hydrochemical baseline by examining Li distribution and its associations with major-ion composition across contrasting water types. In May 2026, water samples were collected from 14 sites, including saline lakes, sors (salt-flat depressions), river reaches, groundwater wells, and a thermal spring. Eight sites were resampled on 30 August 2026; the remaining six were dry or inaccessible. Major ions were determined using titrimetric, turbidimetric and ICP-OES methods, with Li, Na, and K quantified by ICP-OES. Hydrochemical associations in the May dataset ($n = 14$) were evaluated using Spearman rank correlations, permutation tests, and Benjamini–Hochberg false-discovery-rate (FDR) correction. Li^+ concentrations ranged from 0.08 to 0.82 mg L^{-1} in May and from 0.25 to 2.29 mg L^{-1} in August. Concentrations were higher in August at seven of the eight resampled sites. Kishi Oymasha exhibited the highest calculated total dissolved solids (TDS ≈ 275 g L^{-1}) but contained only 0.31 mg L^{-1} Li^+, an indicative value because matrix-specific validation of Li^+ was not performed for the samples with TDS > 100 g L^{-1}. After Benjamini–Hochberg FDR correction of the permutation *p*-values, significant positive associations with Li^+ remained for Cl^-, $Na^+ + K^+$, SO_4^{2-}, and TDS; however, none remained significant when the five May samples with indicative Li^+ results were excluded ($n = 9$). Positive correlations with Ca^{2+}, Mg^{2+}, and total hardness were also observed but were not statistically significant after this correction. These findings suggest that salinity alone does not adequately explain Li distribution. Evaporative concentration, differences in Li supply, hydrological mixing, and water–rock interaction remain competing or complementary hypotheses requiring further investigation using isotopic tracers and site-specific hydrological data.

Keywords: lithium; hydrogeochemistry; saline lakes; salt-flat; thermal groundwater; ion ratios; Mangystau; Kazakhstan

Check for updates

Academic Editor: Maurizio Barbieri

Received: 5 October 2026
Revised: 1 November 2026
Accepted: 2 November 2026
Published: 4 November 2026

Copyright: © 2026 by the authors. Licensee MDPI, Basel, Switzerland. This article is an open access article distributed under the terms and conditions of the Creative Commons Attribution (CC BY) license.

1. Introduction

Lithium (Li) has become a strategically important element because of its central role in rechargeable batteries, energy-storage systems, and emerging low-carbon technologies [1–3]. Rapidly increasing demand has intensified interest in unconventional aqueous Li resources, including groundwater, geothermal and thermal waters, saline lakes, and highly mineralized brines [1–4]. In these systems, Li^+ concentrations are governed by a complex interplay of hydrogeochemical processes, including water–rock interaction, mineral dissolution, evaporation, ion exchange, groundwater circulation, and mixing [5–7]. Accordingly, Li enrichment cannot be reliably interpreted from total dissolved solids (TDS) alone and should instead be evaluated within the broader geological and hydrogeochemical setting.

Studies from major Li-bearing basins worldwide demonstrate that the mechanisms responsible for Li enrichment vary considerably among hydrological and geological environments. In salt lakes of the Qinghai–Tibetan Plateau, Li accumulation is favored by the availability of Li-bearing source material, arid climatic conditions, closed-basin hydrology, and prolonged brine evolution [8]. At Kushui Lake in the western Kunlun Mountains, Li-rich springs were identified as an important source of dissolved Li^+, while evaporation and water mixing further enhanced Li^+ concentrations [9]. Investigations of northern Tibetan salt lakes likewise showed that river recharge and geothermal or cold-spring inputs can contribute differently to Li accumulation, even in geographically adjacent basins [10,11]. In the Tien Shan–Pamir region, the hydrochemical evolution of thermal and mineral waters has been linked to deep groundwater circulation and prolonged water–rock interaction [12]. Together, these studies demonstrate that elevated salinity does not necessarily lead to proportional Li enrichment and that Li distribution reflects the combined influence of source availability, water origin, geological setting, and hydrogeochemical evolution.

Evidence for similar processes has recently emerged from Kazakhstan. Hydrochemical modeling of deep formation waters in the Shu–Sarysu Basin indicated that Li enrichment is associated with water–rock interaction and secondary processes such as evaporite dissolution, dolomitization, and cation exchange [13]. Subsequent field investigations identified highly mineralized Li-bearing Na–Ca–Cl to Ca–Na–Cl brines in deep gas-production wells, confirming the occurrence of Li-bearing subsurface waters in this sedimentary basin [14]. In the Mangystau Region, our previous investigation of formation waters from the Karazhanbas, Zhetybay, and Uzen oil fields revealed Li^+ concentrations of approximately 0.30–1.85 mg L^{-1} [15]. Notably, the most saline waters did not consistently contain the highest Li^+ concentrations, further suggesting that Li occurrence is controlled by specific hydrogeochemical processes rather than by salinity alone [15].

Despite these advances, research in Kazakhstan has focused predominantly on deep formation brines and oilfield waters, whereas the distribution of Li across shallow and surface natural-water systems remains poorly constrained. In the Mangystau Region, an integrated comparison among saline lakes, sors (salt-flat), river waters, groundwater, natural springs, and thermal groundwater within a common regional hydrochemical framework remains lacking. This gap limits understanding of whether Li variability is primarily associated with evaporative concentration or whether other processes, including water–rock interaction, groundwater circulation, hydrological mixing, and differences in water origin, exert stronger influences.

The present study therefore aims to characterize and compare the hydrochemical composition and Li distribution of contrasting surface waters and groundwaters in the Mangystau Region, western Kazakhstan, and to identify the hydrochemical variables associated with Li occurrence. Lithium concentrations are evaluated in relation to physicochemical parameters, TDS, major-ion composition, and ion-to-Li ratios, with attention to differences among water types and between the May and August 2026 sampling dates. The contribution of the study is a first regional hydrochemical baseline that compares several Li-bearing

water environments within a single framework. The data are used to evaluate which explanations—evaporative concentration, differences in Li supply, mixing, and water–rock interaction—are consistent with the observations, rather than to quantify the contribution of individual processes, which would require isotopic tracers and site-specific hydrological data. The results provide a basis for targeted monitoring, source-tracing studies, and the selection of waters for confirmatory sampling.

2. Geological and Hydrogeological Setting

The study area is located in the Mangystau Region of western Kazakhstan, within the South Mangyshlak sedimentary basin. The basin is characterized by a thick and structurally complex sedimentary succession affected by regional uplifts, depressions, folds, and fault systems [16,17]. Mesozoic sedimentary units, particularly Jurassic and Cretaceous deposits, are widely developed and form an important part of the regional geological framework [16,17].

The Zhetybay–Uzen structural zone represents one of the major tectonic elements along the northern margin of the South Mangyshlak depression. The sedimentary succession in this zone reaches approximately 4–5 km in thickness [16]. Jurassic deposits are characterized by heterogeneous terrigenous sequences containing sandstones, siltstones, and clay-rich layers. In the Zhetybay area, Middle Jurassic sandstone bodies show pronounced vertical and lateral heterogeneity related to deltaic depositional environments [17]. The regional geological and tectonic setting and the positions of the sampling sites are shown in Figures 1 and 2.

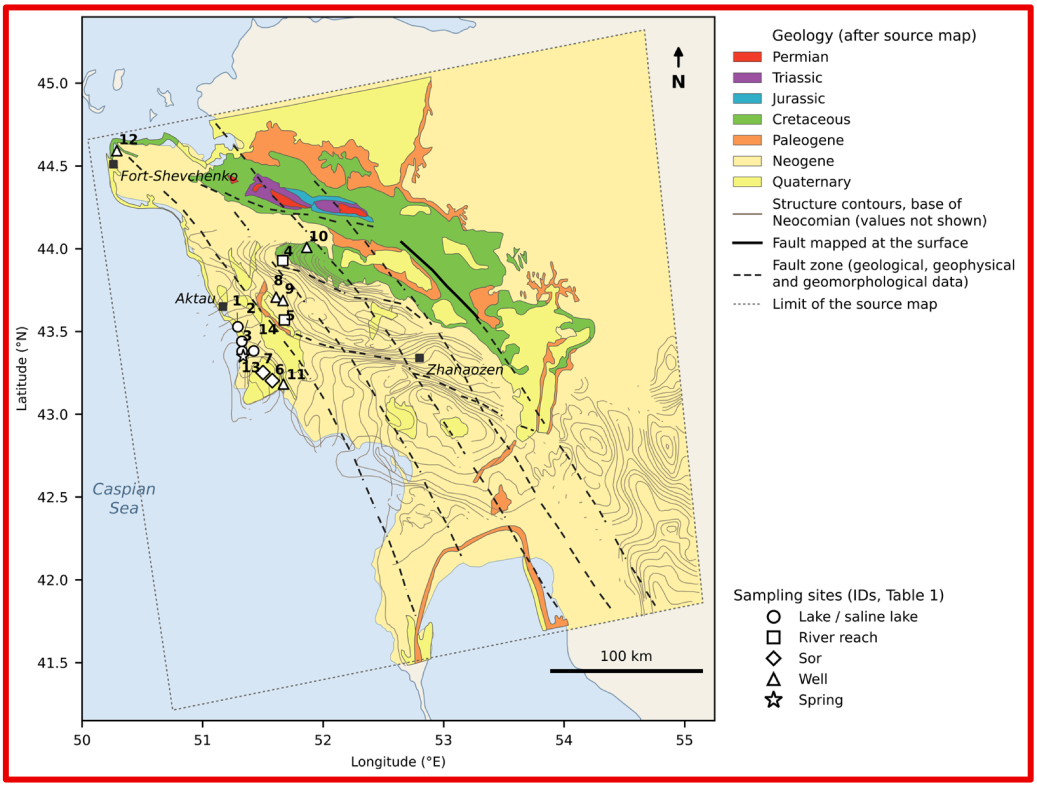


Figure 1. Simplified geological–structural map of South Mangyshlak with the sampling sites (IDs as defined in Section 3.1), redrawn from Figure 27 in Chakabaev et al. [18], a schematic map compiled from materials of VAGT, the trusts Kazakhstanneftegeofizika and Mangyshlakneftegazrazvedka, the Kazakhstanneft association and other organizations. Outcrop units, faults, fault zones and structure contours were digitized by the authors from the georeferenced source map; the structure contours (base of the Neocomian) are shown without their values, and the contours of closed depressions (item 8 of the source legend) were not digitized. Coastline from Natural Earth (1:10 m). The map shows the outcropping units and fault zones around the sampling sites; it was not used in the quantitative analysis.

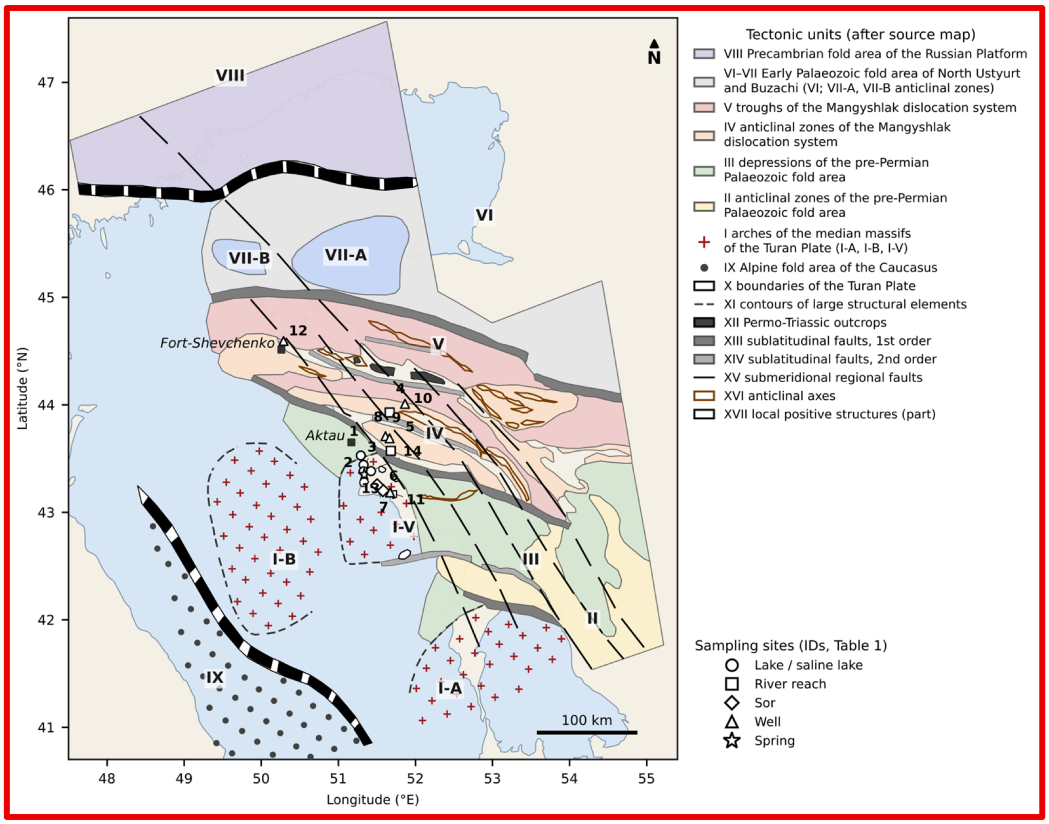


Figure 2. Tectonic scheme of Mangyshlak and adjacent areas with the sampling sites (IDs as defined in Section 3.1), redrawn from Figure 28 in Chakabaev et al. [18], compiled from materials of the trusts Kazakhstanneftegeofizika and Mangyshlakneftegazrazvedka, VAGT, VNIGRI, IGN AN SSSR, OMGR VNIIGeofizika and other organizations. Units of the source legend: I, arches of the median massifs of the Turan Plate (I-A, Karabogazgol arch; I-B, Central Caspian arch; I-V, Peschanomys–Rakushechny block); II–III, area of pre-Permian Palaeozoic folding (II-A, Tuarkyr anticlinal zone; II-B, Kaplankyr (Kumsebshen) anticlinal zone; II-V, Karaudan swell-like uplift; II-G, Karynzharyk saddle; III-A, Segendyk depression; III-B, Kazakh depression; III-G, Ushkuduk–Karasai depression; III-D, Assake–Audan depression); IV–V, Mangyshlak dislocation system (IV-A, Zhetybai–Uzen anticlinal zone; IV-B, Beke–Bashkuduk anticlinal zone; IV-V, Tyub-Karagan anticlinal zone; IV-G, Karatau anticlinal zone; IV-D, Tuzbair anticlinal zone; IV-E, Tumgacha–Karamain anticlinal zone; V-A, Chakyrgan trough; V-B, North Mangyshlak (South Buzachi) trough); VI–VII, area of Early Palaeozoic folding of North Ustyurt and Buzachi (VII-A, North Buzachi anticlinal zone; VII-B, North Kulaly anticlinal zone); VIII, area of Precambrian folding of the Russian Platform; IX, area of Alpine folding of the Caucasus; X, boundaries of the Turan Plate; XI, contours of large structural elements; XII, outcrops of the Permo-Triassic complex; XIII and XIV, sublatitudinal faults of the first and second order; XV, submeridional regional faults; XVI, anticline axes; XVII, local positive structures (only those near Eralievo were digitized). Unit boundaries were digitized by the authors from the georeferenced source scheme; the map shows the tectonic units in which the sampling sites are located.

At depth, prolonged residence of groundwater within sedimentary formations may enhance water–rock interaction and influence the hydrochemical evolution of subsurface waters. The average geothermal gradient of the Mangyshlak Basin is approximately 33 °C km^{-1}, while values close to 32 °C km^{-1} have been reported for the Zhetybay–Uzen structural zone [16]. These regional conditions are relevant to the thermal wells (25–43 °C) sampled in this study; however, without well-construction data they do not establish from which formation each sampled groundwater originates (Section 3.1).

The Mangystau Region has an arid climate with strong evaporation. According to the ERA5 reanalysis [19], accessed through the Open-Meteo Historical Weather API [20] for the

grid cell nearest to Aktau (43.62° N, 51.23° E), mean annual precipitation for 1991–2020 was 163 mm, whereas mean annual FAO-56 reference evapotranspiration (ET_0) [21] was 1276 mm. The first campaign took place in May 2026 (mean May air temperature 17.6 °C; 1991–2020 mean 18.7 °C). The months between the two campaigns were wetter than average: from June to August 2026, precipitation totalled 51 mm, compared with a 1991–2020 mean of 30 mm for these months. Reference evapotranspiration over the same months (590 mm) was close to the 1991–2020 mean (606 mm) and greatly exceeded precipitation, and mean air temperatures in July and August 2026 (27.3 and 27.0 °C) were close to the 1991–2020 means (27.6 and 26.9 °C). Together with the sedimentary setting and the contrasting surface and subsurface water systems, these conditions form the framework in which the observations are interpreted.

3. Materials and Methods

3.1. Sampling Sites, Sample Collection, and Preservation

Water samples were collected from 14 sites across the Mangystau Region, western Kazakhstan, during the first sampling campaign in May 2026. Eight of these sites were resampled on 30 August 2026. The sampling network encompassed contrasting aquatic environments: three locations at Lake Karakol, two reaches of the Ashyagar River, two sors (closed salt-flat depressions containing intermittent shallow brines), the saline lake Kishi Oymasha, five groundwater wells, and a natural thermal spring. The sites were selected to represent a range of hydrogeological and hydrochemical settings and to characterize spatial variability and differences between the two sampling dates. Site identifiers (IDs 1–14) are used consistently throughout the tables, figures, and Supplementary Materials; their locations are shown in Figure 3.

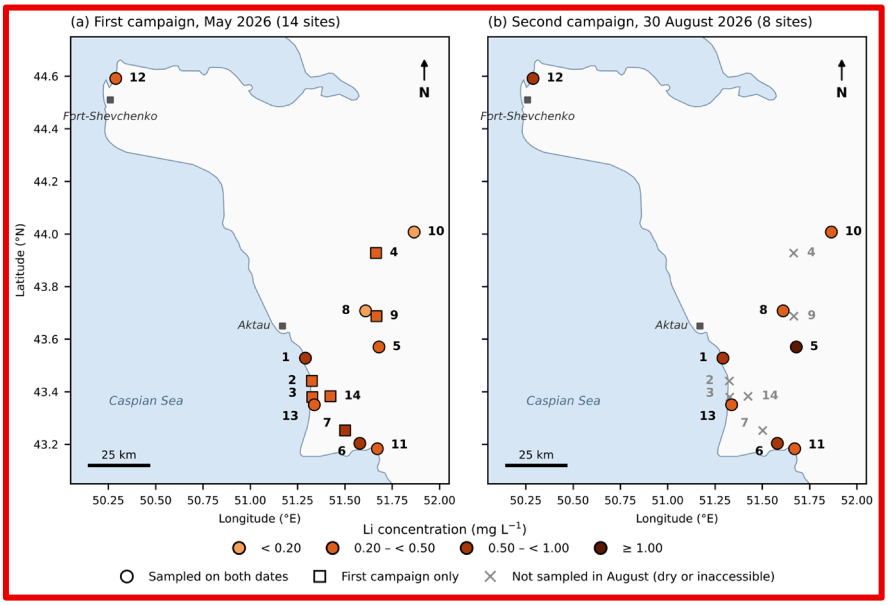


Figure 3. Location of the water-sampling sites (IDs 1–14) in the Mangystau Region, Kazakhstan, and dissolved Li^+ concentrations during (**a**) the first sampling campaign (May 2026; 14 sites) and (**b**) the second sampling campaign (30 August 2026; 8 sites). Li^+ concentrations are displayed using fixed, non-overlapping intervals (<0.20, 0.20–<0.50, 0.50–<1.00, and ≥1.00 mg L^{-1}), with each interval including its lower but excluding its upper boundary. These intervals are descriptive and do not represent geochemical background or anomaly thresholds. Circles indicate sites sampled during both campaigns, whereas squares indicate sites sampled only in May. Grey crosses in panel (**b**) indicate sites that were not sampled in August because they had dried out (IDs 2, 3, 4, 7, and 14) or the well was closed (ID 9). Coastline data were obtained from Natural Earth (1:10 million). Li^+ values of IDs 1, 2, 3, 7 and 14 (May) and ID 5 (August) are indicative (Section 3.3).

Sampling procedures followed established approaches for collecting surface waters, groundwater, and mineralized waters [12,22,23]. Samples from saline lakes and sors were collected directly from the accessible water at the designated sampling locations, whereas samples from the Ashyagar River were obtained directly from flowing river water. Groundwater samples were collected from the continuous discharge streams of permanently operating, pump-equipped wells under normal operating conditions. The wells operated continuously rather than seasonally and were not activated specifically for sampling. No additional well purging was performed because samples were collected from actively flowing water. However, stabilization of physicochemical parameters was not independently documented. Water from the natural thermal spring was collected directly from the accessible discharge. Water temperature was measured in situ using a Testo T1 digital contact thermometer.

Lake Karakol formed when a natural depression was flooded with heated discharge water from the nearby MAEK power plant, which uses Caspian seawater for cooling. The lake is also connected to the Caspian Sea by channels [24,25]. Three samples (Karakol Nos. 1–3) were collected within the lake. Because of the managed seawater supply and potential hydrological connectivity, these sampling locations were treated as anthropogenically influenced and were not assumed to be statistically independent. At Karakol No. 1, Cl^- decreased from 94,430 mg L^{-1} in May to 6923 mg L^{-1} in August (about 14-fold); the calculated sum of major ions decreased from approximately 168 to 13.9 g L^{-1}, but the August value is probably underestimated because the August Na^+ result failed the charge-balance check (Section 3.2). The reason for this difference could not be established from the available field records; therefore, the observed difference was reported without attributing it to a specific hydrological or geochemical mechanism. Available site information, including coordinates, water type, sampling dates, water temperature, and reasons for non-sampling in August, is provided in the Supplementary Materials. Detailed well-construction information, including total depths, screened intervals, aquifer characteristics, and pumping rates, was unavailable. Consequently, groundwater samples were not attributed to specific aquifers or geological formations (Section 5.5).

All 14 sites were sampled in May, whereas only eight were resampled in August. By late summer, Karakol No. 2 (ID 2), Karakol No. 3 (ID 3), the upper reach of the Ashyagar River (ID 4), Ashysor (ID 7), and Kishi Oymasha (ID 14) had dried out, while the Northern Karagiye well (ID 9) was closed and inaccessible. The August subset was therefore not a random sample of the original network. Sites that could not be sampled were treated as missing observations; no zero concentrations or values below the analytical detection limit were assigned.

Water samples were collected in pre-cleaned high-density polyethylene (HDPE) bottles following established procedures for sampling, preservation, handling, transportation, and storage [26]. For each site, geographical coordinates, sampling date and time, sample identification code, water type, and relevant field observations were recorded.

Samples were divided into separate aliquots according to the intended analytical procedures. Aliquots designated for dissolved-element analysis by ICP-OES, including Li, Na, and K, were filtered through 0.45 µm membrane filters and acidified with ultrapure nitric acid (HNO_3) (MF-MilliporeTM, Merck KGaA, Darmstadt, Germany), to pH < 2, following established procedures for dissolved-element determination in water [27]. Separate aliquots intended for Ca^{2+} and Mg^{2+} determination were also preserved by acidification with nitric acid to minimize potential losses caused by carbonate precipitation during storage. Unacidified aliquots were retained for the determination of major anions (CO_3^{2-}, HCO_3^-, Cl^-, and SO_4^{2-}). Samples intended for complexometric determination of Ca^{2+} and Mg^{2+}

were subsequently prepared according to the applicable analytical procedures described in Section 3.2.

All water samples were transported to the laboratory in cooled, insulated containers at approximately 4 ± 2 °C. Physicochemical parameters, major-ion concentrations, and dissolved Li^+ were determined using the analytical procedures described in Sections 3.2 and 3.3. The analytical results for both sampling campaigns are provided in the Supplementary Materials. For Li determination by ICP-OES, 21 of the 22 samples were diluted with deionized water at a sample-to-diluent ratio of 1:1 (dilution factor, DF = 2), whereas the August sample from the lower Ashyagar River reach (ID 5; Li^+ = 2.29 mg L^{-1}) was diluted tenfold (DF = 10). The reported Li^+ concentrations in the original water samples were calculated by correcting the measured concentrations for their respective dilution factors.

3.2. Physicochemical Parameters and Major-Ion Analysis

Physicochemical parameters and major-ion concentrations were determined using standardized hydrochemical procedures. Water temperature was measured in situ at the time of sampling using a Testo T1 digital contact thermometer (Testo SE & Co. KGaA, Titisee-Neustadt, Germany). Measurements were obtained at all 14 sites in May and at the eight sites sampled in August. Temperatures are reported to 0.1 °C; statistical calculations used the recorded values listed in the Supplementary Materials.

pH was measured potentiometrically using a calibrated pH-150MI pH meter (WTW, Weilheim, Germany) in accordance with ST RK ISO 10523-2013. pH was measured in the laboratory during the analytical period, i.e., several days after sampling. Laboratory analyses were conducted at an ambient temperature of 24.0–25.1 °C and a relative humidity of 50–55%. Because CO_2 degassing between sampling and analysis may shift pH, particularly in the thermal waters, pH is used only descriptively.

Total dissolved solids (TDS; referred to as mineralization in the Russian-language hydrochemical literature) were calculated as the sum of the measured major-ion concentrations (CO_3^{2-}, HCO_3^-, Cl^-, SO_4^{2-}, Ca^{2+}, Mg^{2+} and $Na^+ + K^+$); the term TDS is used throughout the text. Carbonate (CO_3^{2-}) was not detected in any sample (Supplementary Materials) and was therefore not included in the numerical sum used to calculate TDS. Accordingly, TDS was calculated as the sum of the reported concentrations of HCO_3^-, Cl^-, SO_4^{2-}, Ca^{2+}, Mg^{2+}, and $Na^+ + K^+$. No independent gravimetric determination of TDS was performed. Because calculated TDS is not independent of the major ions from which it is derived, correlations of Li^+ with TDS and with individual major ions are not treated as independent lines of evidence (Section 5.1).

The Kishi Oymasha sample (ID 14) had a calculated TDS of approximately 274.98 g L^{-1}, derived from the sum of the reported major-ion concentrations. This value is an estimate of mineralization and was not independently confirmed by direct gravimetric measurement; it should not be interpreted as a separately measured TDS result.

Total hardness was determined by EDTA complexometric titration according to GOST 26449.1-85, Section 10, for the August samples and expressed in meq L^{-1}. For the May campaign, total hardness values used in the statistical analysis and in Section 4.4 were calculated from the reported Ca^{2+} and Mg^{2+} concentrations (Ca^{2+}/20.04 + Mg^{2+}/12.15, expressed in meq L^{-1}). Mg^{2+} concentrations below the detection limit were treated as zero for this calculation, contributing a maximum difference of less than 0.17 meq L^{-1}. The originally reported May hardness values (from the authors' original data compilation), which differ from the recalculated values for some samples (e.g., IDs 2 and 13), are listed separately from the recalculated values in the Supplementary Materials. Calcium (Ca^{2+}) and magnesium (Mg^{2+}) were determined by EDTA complexometric titration in accordance with Sections 11.1 and 12, respectively. Carbonate (CO_3^{2-}) and bicarbonate (HCO_3^-)

were determined by sequential acid–base titration according to Section 7, while chloride (Cl^-) was determined argentometrically using standardized $AgNO_3$ in accordance with Section 9.1. Comparable standardized hydrochemical procedures have also been applied in recent groundwater studies in western Kazakhstan [28].

According to GOST 26449.1-85 [29], the complexometric determinations of Ca^{2+} and Mg^{2+} are applicable from 20 mg L^{-1}, with lower detection limits of 3.0 and 2.0 mg L^{-1}, respectively (Sections 11.1 and 12.1). Because Mg^{2+} is obtained from the difference between the Ca + Mg and Ca titrations, its uncertainty increases at low Mg/Ca ratios. Mg^{2+} results below 2.0 mg L^{-1} are therefore reported as censored values (<2.0 mg L^{-1}), and results between 2.0 and 20 mg L^{-1} are flagged as semi-quantitative (Section 4.4). The laboratory reports confirm that Mg^{2+} was determined by this method.

Sulfate (SO_4^{2-}) was determined turbidimetrically: $BaSO_4$ is precipitated and the resulting turbidity is read photometrically. For the August samples, a DR 2800 spectrophotometer (Hach, Loveland, CO, USA) was used with the SulfaVer 4 reagent (Hach Method 8051 [30]); for the first-campaign samples, the laboratory used method MVI No. 6-10. Highly mineralized samples were diluted as necessary to maintain sulfate concentrations within the working range of the method, and reported concentrations were corrected for the respective dilution factors; check-standard results for sulfate were not reported by the laboratory. Gravimetric determination, which would be preferable for the most sulfate-rich samples, was not performed.

The analytical consistency of the major-ion data was evaluated with the charge-balance error, CBE (%) = 100 × (Σcations − Σanions)/(Σcations + Σanions), with all concentrations in meq L^{-1}. For the first campaign, for which only $Na^+ + K^+$ is available, this sum was converted to meq L^{-1} as Na; in August, Na^+ and K^+ were converted separately. For the nine first-campaign samples for which the original laboratory reports are available, the CBE ranged from −11.4% to +15.8% and was within ±5% for six samples; it was −5.3% for Ashysor Lower (ID 6), −11.4% for Ashysor (ID 7) and +15.8% for the 14th Siding well (ID 10). Because $Na^+ + K^+$ was converted as Na, these values are approximate; the imbalance does not, by itself, indicate an error in the Li^+ results. The nonzero CBE values indicate departures from exact ionic charge balance but do not, by themselves, establish whether $Na^+ + K^+$ was determined independently or calculated by difference. For the five first-campaign samples for which the original laboratory reports were unavailable (IDs 8, 11, 12, 13, and 14), the CBE ranged from +2.0% to +3.1% for IDs 8, 11, and 12. The calculated CBE was zero for Radon Spring (ID 13) and Kishi Oymasha (ID 14), which is consistent with $Na^+ + K^+$ having been obtained by difference. However, the original analytical records are unavailable to confirm the method used to obtain these values.

In the August campaign, the CBE ranged from −64% to +25% and exceeded 10% in seven of the eight samples, while the reported Na^+ concentrations (763–2200 mg L^{-1}) varied little with salinity (Cl^- 932–84,300 mg L^{-1}). The August Na^+ data are therefore regarded as unreliable for quantitative hydrochemical interpretation. Consequently, Na-dependent hydrochemical indicators and Sulin water types are not interpreted for August, whereas the calculated CBE values are retained to document analytical consistency. The absolute CBE values of the August analyses, in which Na^+ and K^+ were reported separately, are therefore much larger than those of the May analyses, in which $Na^+ + K^+$ was reported as one value. In August, the CBE was negative (anion excess) in seven of the eight samples, which is consistent with underestimated Na^+ concentrations. The difference between the campaigns may largely reflect inaccuracies in the August Na^+ results rather than differences in how Na^+ and K^+ were reported. For the May analyses, a partial adjustment of $Na^+ + K^+$ to the ionic balance, as suggested by the zero CBE of IDs 13 and 14, would also lower the CBE, but this cannot be verified without the original analytical records.

3.3. ICP-OES Analysis and Quality Control

Lithium (Li), sodium (Na), and potassium (K) concentrations were determined by inductively coupled plasma optical emission spectrometry (ICP-OES) using a Shimadzu ICPE-9000 spectrometer (Shimadzu Corporation, Kyoto, Japan), following the validated analytical procedure previously applied to highly mineralized waters from the Mangystau Region [15]. Measurements were performed in axial observation mode using high-purity argon. The radio-frequency power was set to 1.20 kW, and the plasma, auxiliary, and carrier-gas flow rates were 10.0, 0.60, and 0.70 L min^{-1}, respectively. The exposure time was 30 s.

Lithium was quantified at an analytical wavelength of 670.784 nm using external calibration over the concentration range of 0.03125–1.00 mg L^{-1}. The calibration curve showed good linearity ($R^2 = 0.99967$). The instrumental limit of detection (LOD), calculated as $3\sigma/s$, was 0.001 mg L^{-1}, and the instrumental limit of quantification (LOQ), calculated as $10\sigma/s$, was 0.003 mg L^{-1}, where σ represents the standard deviation of the blank signal and s is the slope of the calibration curve. For routine data reporting, a practical quantification limit of 0.03125 mg L^{-1}, corresponding to the lowest calibration standard, was adopted. This limit refers to the concentration in the measured (diluted) solution; the effective quantification limit in the original water equals 0.03125 mg L^{-1} multiplied by the dilution factor. Based on the specified dilution factors, the effective practical quantification limit in the original waters was 0.0625 mg L^{-1} for the 21 samples with DF = 2 and 0.3125 mg L^{-1} for the sample with DF = 10. These limits address calibration-range quantification, not matrix-specific accuracy. The effective instrumental LOD and LOQ in the original water were 0.002 and 0.006 mg L^{-1} for DF = 2, respectively, and 0.010 and 0.030 mg L^{-1} for DF = 10, respectively.

All 22 samples were diluted before Li measurement: 21 using DF = 2 and one August sample (lower Ashyagar River reach, ID 5) using DF = 10. The measured Li concentrations in the diluted analytical solutions for the 21 twofold-diluted samples ranged from 0.040 to 0.410 mg L^{-1}, within the calibration range of 0.03125–1.00 mg L^{-1}. One sample collected during the August campaign exceeded the upper calibration limit and was diluted tenfold. The final Li^+ concentration, after correction for the dilution factor, was 2.29 mg L^{-1} (i.e., 0.229 mg L^{-1} in the measured solution). EPA Method 200.7 recommends dissolved-solids content below 0.2% (w/v) in the measured solution to reduce interference [27]. The twofold dilution of the Kishi Oymasha sample would yield a calculated dissolved-solids concentration of approximately 137.49 g L^{-1}, markedly exceeding that guidance; therefore, calibration-range compliance alone does not demonstrate that the Li measurement was free from matrix effects. For Kishi Oymasha, the calculated dissolved-solids loading after dilution is approximately 68.7 times the 2 g L^{-1} guidance threshold; this ratio quantifies potential matrix loading, not analytical bias or lithium recovery.

For the first campaign, the laboratory reported Na^+ and K^+ only as a combined value ($Na^+ + K^+$); individual Na^+ and K^+ concentrations are not available. In August, Na^+ and K^+ were determined separately by ICP-OES and are also reported as their sum for comparison; however, the August Na^+ results did not pass the charge-balance check (Section 3.2).

Analytical quality assurance and quality control (QA/QC) included procedural blanks, replicate measurements, an independent quality-control sample (IQC) prepared from a second-source certified Li standard, a continuing calibration blank (CCB), and a continuing calibration verification (CCV) standard. Acceptance criteria were set at ±20% of the nominal concentration for the IQC and ±15% for the CCV. A certified reference material (CRM) was also used as part of the laboratory quality-control procedure; because sample-matrix-specific CRM recovery data were not available, this control cannot be interpreted as a direct assessment of recovery in the Kishi Oymasha brine.

The CCV standard, with a nominal Li^+ concentration of 0.0625 mg L^{-1}, yielded measured concentrations of 0.0644 and 0.0687 mg L^{-1} at the beginning and end of the analytical sequence, corresponding to recoveries of 103.0% and 109.9%, respectively. The IQC standard, with a nominal concentration of 0.125 mg L^{-1}, yielded 0.135 mg L^{-1}, corresponding to a recovery of 108.0%. Replicate measurements produced relative standard deviations (RSDs) ranging from 0.24% to 3.16%, demonstrating satisfactory analytical precision. The laboratory did not report whether these QC results refer to one or to both analytical sequences, so QC results for the two campaigns cannot be given separately. All three QC recoveries exceeded 100% (103.0–109.9%), suggesting a possible positive systematic bias of up to approximately 10% in the reported Li^+ concentrations; the data were not corrected for this potential bias. If this bias were constant and proportional across all samples, it would not affect the Spearman rank correlations or the ranking of the samples. However, the possible bias should be considered when comparing absolute Li^+ concentrations with those reported in other studies. For illustration, correcting the August maximum of 2.29 mg L^{-1} for a hypothetical positive bias of 10% would yield approximately 2.08 mg L^{-1} (2.29/1.10), which would still exceed the maximum of 1.85 mg L^{-1} reported for regional formation waters [15]. This illustrative correction does not account for potential sample-specific matrix effects.

Matrix-spike recovery tests were not performed during the present analytical sequence. Instead, analytical accuracy, calibration stability, potential contamination, and measurement repeatability were assessed using the second-source IQC, CCV, CCB, procedural blanks, and replicate analyses in accordance with the laboratory QA/QC procedure and established ICP-OES analytical practice [27]. These checks do not establish analyte recovery in the sample matrix; matrix effects in the most saline samples therefore cannot be excluded, and Li^+ results for the samples with TDS > 100 g L^{-1} (IDs 1, 2, 3, 7 and 14 in May and ID 5 in August) are regarded as indicative. The threshold of 100 g L^{-1} is operational: it separates the five most mineralized May samples (TDS 138–275 g L^{-1}) from the remaining May samples (TDS $\leq$ 82 g L^{-1}) and was not derived from a measured matrix effect. Samples below this threshold were not matrix-validated either: after twofold dilution, all May samples except IDs 8 and 10 (TDS 2.93 and 2.89 g L^{-1}) also exceeded the 2 g L^{-1} (0.2%) dissolved-solids guidance of EPA Method 200.7 [27], so their Li^+ results are also subject to a possible matrix effect, which is expected to be smaller. Calibration checks and statistical sensitivity analyses do not replace validation in the sample matrix.

For Kishi Oymasha (ID 14), the reported Li^+ concentration of 0.31 mg L^{-1} corresponds to 0.155 mg L^{-1} in the analytical solution after DF = 2, which lies within the established calibration range. However, the sample-specific effect of its highly saline matrix was not independently verified using standard additions, matrix-matched calibration, or matrix-spike recovery. Accordingly, this Li^+ result is treated as indicative and subject to possible matrix-related uncertainty; the calculated TDS value does not in itself validate the Li determination. Additional matrix-specific analytical verification would be required to confirm its quantitative accuracy. No numerical matrix-spike recovery or matrix-induced percentage bias is reported because no corresponding experimental measurements were performed.

3.4. Cartographic and Spatial Analysis

The geological–structural map and the tectonic scheme (Figures 1 and 2) were redrawn from Figures 27 and 28 of Chakabaev et al. [18]. The scanned source figures were georeferenced in QGIS 3.44.7 "Solothurn" to WGS 84 (EPSG:4326) using ground control points, and stratigraphic units, structure contours, faults, fault zones and tectonic units were digitized as vector layers. The final maps were drawn from these vector layers with Python 3.13 using GeoPandas 1.2, Shapely 2.2, matplotlib 3.11 and adjustText 1.4, together with the coastline from Natural Earth (1:10 m) and the sampling sites.

The sampling map (Figure 3) was drawn with the same software from the field-recorded coordinates of the sites (WGS 84, EPSG:4326; Supplementary Materials) on the Natural Earth coastline at a scale of 1:10,000,000. Li^+ concentrations are shown separately for each campaign in fixed concentration intervals (<0.20, 0.20–<0.50, 0.50–<1.00 and ≥1.00 mg L^{-1}); these intervals are descriptive and do not represent background or anomaly thresholds. Site labels were placed manually to avoid overlap, and Figures 1–3 were exported at 600 dpi.

The spatial dataset included all 14 sampling locations. Sites that were unavailable during the August campaign were retained on the map, with a different symbol, to represent the complete sampling network and to document the contraction of the surface-water network by August.

Because the sampling network comprised only 14 spatially non-uniform locations, spatial interpolation methods, including inverse distance weighting (IDW), kriging, and related approaches, were not applied. Consequently, the maps show the actual sampling locations and measured analytical data rather than interpolated or predicted concentration surfaces.

3.5. Hydrochemical and Statistical Data Analysis

Hydrochemical and statistical analyses were performed to characterize the investigated waters, evaluate associations between Li^+ and major hydrochemical variables, and compare the May and August 2026 results at the resampled sites.

Descriptive statistics were calculated for Li^+, TDS, pH, water temperature, total hardness, and major-ion concentrations. Associations between Li^+ and TDS, Cl^-, SO_4^{2-}, Ca^{2+}, Mg^{2+}, HCO_3^-, total hardness, $Na^+ + K^+$, pH, and water temperature were evaluated for the May dataset ($n = 14$) using Spearman's rank correlation coefficient (ρ). Spearman correlation was selected as the primary measure because of the limited sample size, the broad hydrochemical range represented by the contrasting water types, and the potential influence of non-normal distributions and extreme values.

Two-sided p-values were obtained in two ways: from the asymptotic t-approximation implemented in scipy.stats.spearmanr, and from a Monte Carlo permutation test in which the pairing between Li^+ and each variable was broken by randomly permuting the ranks of Li^+ (99,999 permutations, random seed 20261022; p = (number of $|\rho_{perm}| \geq |\rho_{obs}| + 1)/(99{,}999 + 1)$). Tied values were assigned mid-ranks, and censored values (e.g., $Mg^{2+} < 2.0$ mg L^{-1}) were treated as tied below the lowest detected value. To account for multiple testing across the ten variables, both sets of p-values were adjusted with the Benjamini–Hochberg false-discovery-rate (FDR) procedure [31]. Associations were considered statistically significant when the FDR-adjusted p-value was <0.05.

Statistical analyses were performed in Python 3.13.5 using pandas 2.2.3, NumPy 2.3.5, and SciPy 1.17.0, including functions from the scipy.stats module. Given the limited number of observations and the marked hydrochemical heterogeneity among the investigated water types, correlation coefficients were interpreted together with scatter plots and individual sample characteristics rather than solely on the basis of statistical significance. Robustness and uncertainty were evaluated descriptively by (i) repeating the correlations separately for surface waters ($n = 8$) and for groundwater wells and the spring ($n = 6$); (ii) a leave-one-out analysis recording the range of ρ when each site was removed in turn; (iii) repeating the correlations with Lake Karakol represented by a single point (ID 1); (iv) repeating the correlations without the five May samples whose Li^+ results are regarded as indicative (IDs 1, 2, 3, 7 and 14; $n = 9$; Section 3.3), with permutation p-values and FDR correction as for the complete dataset; and (v) percentile bootstrap 95% confidence intervals for ρ (9999 resamples of sites, same seed).

Dissolved constituents are written as ions (e.g., Li^+, Na^+, Ca^{2+}, Cl^-) where their concentrations are referred to, whereas element symbols without charges are used for ratios (e.g., Mg/Li, Li/Cl), isotopes and analytical determinations. Selected ion-to-Li mass

ratios, including Mg/Li, Ca/Li, (Na + K)/Li, Cl/Li, and SO_4/Li, were calculated from concentrations expressed in mg L^{-1} and used as comparative indicators of the hydrochemical conditions associated with Li occurrence. The corresponding equivalent ratios are obtained by multiplying the Mg/Li and Ca/Li mass ratios by 0.571 and 0.346, respectively (equivalent masses of Li, Mg and Ca: 6.94, 12.15 and 20.04 g eq^{-1}); because these factors are constant, the ranking of the samples is the same for mass and equivalent ratios. Individual Na/Li and K/Li ratios were calculated only for samples in which Na^+ and K^+ were determined separately. The Li/Cl mass ratio (given as 10^5 × Li/Cl in Section 4.4) was also calculated, because it remains constant when a water in which Li and Cl behave conservatively (i.e., before halite saturation) is concentrated by evaporation or diluted; departures from a constant ratio therefore indicate additional Li supply or removal, or mixing with water of different Li/Cl. Differences between May and August were evaluated for the eight sites sampled on both dates. For each parameter, the absolute May–August change was calculated as

$$\Delta C = C_{\mathrm{Aug}} - C_{\mathrm{May}} \quad (1)$$

and the relative May–August change was calculated as

$$\Delta \boldsymbol{C}(\%) = \frac{\boldsymbol{C_{\mathrm{Aug}} - C_{\mathrm{May}}}}{\boldsymbol{C_{\mathrm{May}}}} \times 100 \quad (2)$$

where C_{May} and C_{Aug} represent values of the same hydrochemical parameter measured at the same sampling site in May and August 2026, respectively. Positive values indicate an increase from May to August, whereas negative values indicate a decrease. Sites that could not be sampled in August were treated as missing observations and excluded from paired calculations.

Hydrochemical water types were assigned with the genetic classification of Sulin [32], which uses ratios of equivalent concentrations: waters with rNa/rCl > 1 are sulfate–sodium if $(rNa - rCl)/rSO_4 < 1$ and bicarbonate–sodium if this ratio exceeds 1, whereas waters with rNa/rCl < 1 are chloride–magnesium if $(rCl - rNa)/rMg < 1$ and chloride–calcium if this ratio exceeds 1; here rNa denotes $Na^+ + K^+$ in meq L^{-1}. Scatter plots of Li^+ against the principal hydrochemical variables were generated using matplotlib 3.11 and NumPy 2.3.5.

Given the small number of paired observations ($n = 8$) and the marked hydrochemical heterogeneity of the investigated waters, May–August comparisons were treated as exploratory and descriptive; two sampling dates in one year cannot establish a recurring seasonal cycle. Correlations and ion-to-Li ratios were interpreted as indicators of hydrochemical associations rather than as direct evidence of individual geochemical processes. Potential controls on Li occurrence—including evaporation, dilution, water mixing, groundwater circulation, and water–rock interaction—were therefore evaluated by integrating the statistical results with hydrochemical, hydrological, and geological evidence.

4. Results

4.1. Field Conditions and Physicochemical Characteristics

The investigated waters represented contrasting surface and subsurface environments, including saline lakes, rivers, salt-flat, groundwater wells, and natural springs. All 14 sites were sampled during the first campaign in May 2026, whereas only eight sites could be resampled in August. By late summer, five surface-water sites had dried out, while the Northern Karagiye well was inaccessible.

Water temperatures varied markedly among the investigated water types. Surface waters generally exhibited lower temperatures during the May campaign, whereas groundwater wells and springs were considerably warmer. The highest temperatures were recorded in the 14th Siding well and Radon Spring, reaching 40.2 and 41.2 °C in May, respectively. In August, Radon Spring reached 43.4 °C and the 14th Siding well 41.1 °C. In May, all eight surface

waters were between 9.5 and 13.4 °C, whereas the five groundwater wells and the spring were between 25.1 and 41.2 °C, so that temperature mainly separates the two hydrological regimes.

Lithium concentrations ranged from 0.08 to 0.82 mg L^{-1} in May and from 0.25 to 2.29 mg L^{-1} at the eight resampled sites in August. The highest May concentration occurred at Ashysor Lower (ID 6; 0.82 mg L^{-1}), whereas the maximum August concentration was measured in the lower Ashyagar reach (ID 5; 2.29 mg L^{-1}).

The warmest waters were not necessarily the most Li-rich. In May, Radon Spring (ID 13) contained 0.24 mg L^{-1} Li^+ at 41.2 °C, whereas the much cooler Ashysor Lower (ID 6) contained 0.82 mg L^{-1} Li^+ at 12.0 °C. Lithium concentrations and water temperatures at all sites on both dates are shown in Figure 4 and listed in Table 1.

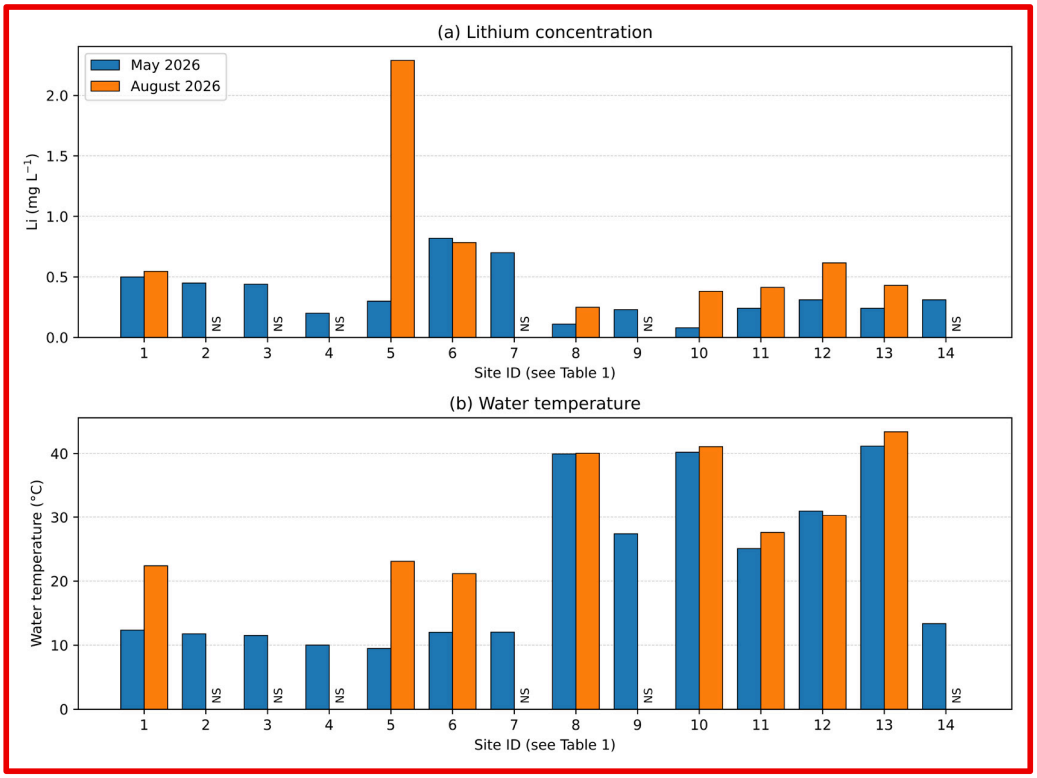


Figure 4. Lithium concentrations (**a**) and water temperatures (**b**) in May and August 2026. **Note:** Site IDs correspond to Table 1. NS = not sampled in August (site dry: IDs 2, 3, 4, 7 and 14; well closed: ID 9); missing observations do not represent zero values. Li^+ values of IDs 1, 2, 3, 7 and 14 (May) and ID 5 (August) are indicative (Section 3.3).

Table 1. Water temperature and lithium concentrations at the investigated sites on the two sampling dates.

Site ID	Sampling Site	Water Type	T, May (°C)	Li^+, May (mg L^{-1})	T, August (°C)	Li^+, August (mg L^{-1})
1	Karakol No. 1	Lake [a]	12.4	0.50	22.4	0.55
2	Karakol No. 2	Lake [a]	11.8	0.45	—	—
3	Karakol No. 3	Lake [a]	11.5	0.44	—	—
4	Ashyagar, upper reach	River	10.0	0.20	—	—
5	Ashyagar, lower reach	River	9.5	0.30	23.1	2.29
6	Ashysor Lower	Sor	12.0	0.82	21.2	0.78
7	Ashysor	Sor	12.0	0.70	—	—
8	Ashyagar–Alatobe	Well	40.0	0.11	40.1	0.25

Table 1. *Cont.*

Site ID	Sampling Site	Water Type	T, May (°C)	Li^+, May (mg L^{-1})	T, August (°C)	Li^+, August (mg L^{-1})
9	Northern Karagiye	Well	27.4	0.23	—	—
10	14th Siding	Well	40.2	0.08	41.1	0.38
11	Kuryk (Eralievo F-1)	Well	25.1	0.24	27.6	0.41
12	Sad Dubsky F-1	Well	31.0	0.31	30.3	0.62
13	Radon Spring	Spring	41.2	0.24	43.4	0.43
14	Kishi Oymasha	Saline lake	13.4	0.31	—	—

— not sampled in August (site dry: IDs 2, 3, 4, 7, 14; well closed: ID 9); these are missing observations, not zero values. Temperatures are rounded to 0.1 °C (recorded values in the Supplementary Materials) and August Li^+ values to 0.01 mg L^{-1}. [a] Lake Karakol is an artificial water body fed by power-plant cooling water drawn from the Caspian Sea [24,25]; points 1–3 were sampled within the lake. Li^+ values of IDs 1, 2, 3, 7 and 14 (May) and ID 5 (August) are indicative (TDS > 100 g L^{-1}; Section 3.3).

4.2. Lithium Distribution and Differences Between May and August

In May, Li^+ concentrations ranged from 0.08 to 0.82 mg L^{-1}. The highest concentration was measured in Ashysor Lower (ID 6; 0.82 mg L^{-1}), followed by Ashysor (ID 7; 0.70 mg L^{-1}), whereas the lowest concentration occurred in the 14th Siding well (ID 10; 0.08 mg L^{-1}).

In August, Li^+ concentrations at the eight resampled sites ranged from 0.25 to 2.29 mg L^{-1}. Li^+ was higher in August than in May at seven of the eight sites; the median paired difference was +0.18 mg L^{-1} (range −0.04 to +1.99 mg L^{-1}; Figures 4a and 5). At the three resampled surface-water sites, the changes were +0.05 mg L^{-1} (+9%) at Karakol No. 1, +1.99 mg L^{-1} (+663%) in the lower Ashyagar reach, and −0.04 mg L^{-1} (−4%) at Ashysor Lower; the last change is small relative to the combined analytical and sampling uncertainty and is not interpreted as an opposite response. At the four wells and the spring, Li^+ increased by 0.14–0.31 mg L^{-1} (+72% to +376%), while Cl^- changed by only −4% to +17% and water temperature by −0.7 to +2.5 °C. Differences and percentages are calculated from the unrounded August laboratory values (e.g., 0.546 and 0.784 mg L^{-1} at IDs 1 and 6), which are listed in the Supplementary Materials together with the May values.

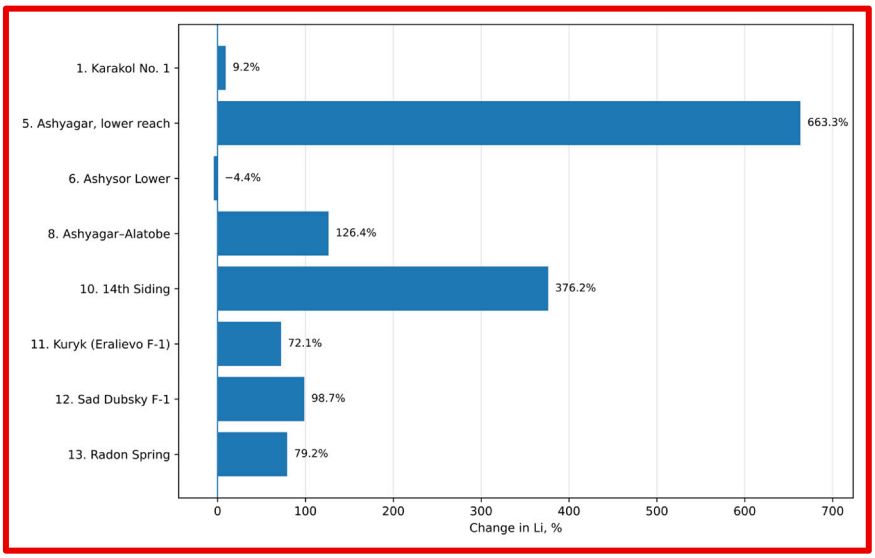


Figure 5. Relative change in Li^+ concentration between May and August 2026 at the eight sites sampled on both dates (site IDs as in Table 1). Positive values indicate an increase; values are calculated from the unrounded laboratory results. The values for IDs 1 and 5 involve indicative Li^+ results (Section 3.3).

The August concentration of 2.29 mg L^{-1} in the lower Ashyagar reach was the highest value measured in this study and slightly exceeded the maximum Li^+ concentration found in our previous study of formation waters from the Karazhanbas, Zhetybay and Uzen oil fields (1.85 mg L^{-1}) [15]. The flow condition of the lower reach at the time of August sampling was not documented; its Cl^- concentration was 84,313 mg L^{-1}, compared with 46,150 mg L^{-1} in the first campaign; the August TDS of this sample (Supplementary Materials) is not interpreted because its Na^+ result failed the charge-balance check (Section 3.2). Because this value is based on a single sample, analytical confirmation and repeated field sampling are required to establish whether it represents a persistent feature or a transient condition.

4.3. Major-Ion Composition and Relationships with Lithium

The hydrochemical composition of the investigated waters was heterogeneous. According to the Sulin classification [32] (Section 3.5), the first-campaign samples, with $Na^+ + K^+$ expressed as Na (Section 3.3), were of the sulfate–sodium (IDs 1–4, 6, 7, 9 and 13), bicarbonate–sodium (IDs 5, 8, 10, 11 and 12) or chloride–magnesium type (Kishi Oymasha, ID 14). For IDs 1–4 and 6, however, rNa/rCl was only 1.015–1.022; because K^+ is included in the $Na^+ + K^+$ value, the true rNa/rCl may be below 1, so the sulfate–sodium assignment of these samples is uncertain. For IDs 13 and 14, the zero CBE is consistent with $Na^+ + K^+$ having been obtained by difference, but this cannot be confirmed from the available records (Section 3.2). The August samples were not classified, because their Na^+ data failed the charge-balance check (Section 3.2); the change from predominantly sulfate–sodium to chloride–calcium types reported in the original submission is therefore not interpreted. In May, TDS ranged from 2.89 to 274.98 g L^{-1}, spanning low-mineralized groundwater and hypersaline surface waters.

The highest TDS did not correspond to the highest Li^+ concentration. Kishi Oymasha (ID 14) had the highest TDS in the dataset (274.98 g L^{-1}) but contained only 0.31 mg L^{-1} Li^+ (an indicative value; Section 3.3), whereas Ashysor Lower (ID 6) contained 0.82 mg L^{-1} Li^+ at a TDS of 23.95 g L^{-1}.

The Li–TDS relationship in May is shown in Figure 6. Although Li^+ generally increased with TDS, the relationship was not proportional, as shown by the wide scatter of the data points and the distinct position of Kishi Oymasha (ID 14). A single proportional Li–TDS relationship therefore does not describe all investigated waters.

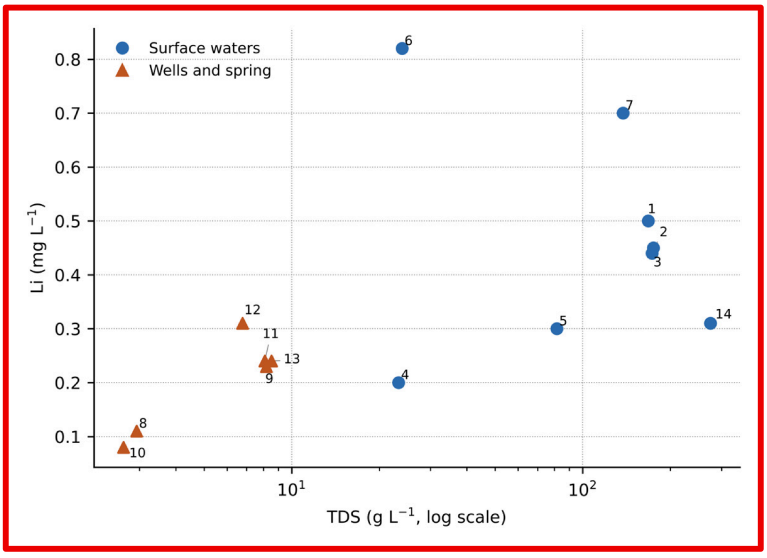


Figure 6. Relationship between Li^+ concentration and TDS in May 2026 (n = 14). The TDS axis is logarithmic; point labels are site IDs (Table 1). Circles: surface waters; triangles: wells and the spring. Li^+ values of IDs 1, 2, 3, 7 and 14 are indicative (Section 3.3).

The statistical relationships between Li^+ and selected hydrochemical parameters are summarized in Table 2.

Table 2. Spearman rank correlations between Li^+ and selected hydrochemical variables in May 2026 ($n = 14$).

Parameter	Spearman ρ	p_{asym}	FDR p_{asym}	p_{perm}	FDR p_{perm}
Cl^-	0.729	0.0031	0.0142	0.0042	0.0172
$Na^+ + K^+$	0.722	0.0035	0.0142	0.0046	0.0172
SO_4^{2-}	0.700	0.0053	0.0142	0.0066	0.0172
TDS	0.696	0.0057	0.0142	0.0069	0.0172
Ca^{2+}	0.564	0.0357	0.0549	0.0386	0.0594
Total hardness	0.557	0.0384	0.0549	0.0416	0.0594
Mg^{2+} [a]	0.568	0.0342	0.0549	0.0384	0.0594
pH	0.536	0.0483	0.0604	0.0508	0.0635
Water temperature	−0.456	0.1013	0.1126	0.1040	0.1156
HCO_3^-	0.235	0.4190	0.4190	0.4163	0.4163

All tests are two-sided. p_{asym}: asymptotic *p*-value (scipy.stats.spearmanr); p_{perm}: Monte Carlo permutation *p*-value (99,999 permutations, seed 20261022). FDR: *p*-values adjusted for the ten comparisons with the Benjamini–Hochberg procedure [31], applied separately to p_{asym} and p_{perm}. Associations with FDR-adjusted $p < 0.05$ are considered statistically significant. [a] Five Mg^{2+} values below the 2.0 mg L^{-1} detection limit were ranked as ties below the lowest detected value (Section 3.5). The Li^+ results of IDs 1, 2, 3, 7 and 14 are indicative (Section 3.3); without these samples ($n = 9$), no association remains significant after FDR correction (Section 4.3).

After Benjamini–Hochberg FDR correction of the permutation *p*-values, statistically significant positive associations with Li^+ remained for Cl^- (ρ = 0.729), $Na^+ + K^+$ (ρ = 0.722), SO_4^{2-} (ρ = 0.700), and TDS (ρ = 0.696), with FDR-adjusted permutation *p*-values of 0.0172 for all four variables (Table 2). Positive correlations were also observed for Ca^{2+} (ρ = 0.564), Mg^{2+} (ρ = 0.568), and total hardness (ρ = 0.557); however, these associations did not remain statistically significant after permutation-based FDR correction (FDR-adjusted pperm = 0.0594). These variables covary with salinity, and TDS is calculated from the same major ions. Therefore, the significant correlations should be interpreted as a common salinity-related association rather than independent evidence of specific hydrogeochemical processes. The Mg^{2+} association should be interpreted cautiously because five Mg^{2+} concentrations were below the detection limit of the titrimetric method and were treated as tied ranks in the statistical analysis (Sections 3.2 and 3.5).

pH (ρ = 0.536) was nominally significant only with the asymptotic test ($p = 0.048$; $p_{perm} = 0.051$) and not after FDR correction, and no association was observed between Li^+ and HCO_3^- (ρ = 0.235). Water temperature showed a moderate negative rank relationship with Li^+ (ρ = −0.456; bootstrap 95% CI −0.85 to 0.13; $p_{perm} = 0.104$), but this relationship was not statistically significant. Because temperature separates the surface waters (9.5–13.4 °C) from the groundwater wells and the spring (25.1–41.2 °C), the pooled coefficient mainly reflects this contrast: within the two groups, ρ was +0.524 for surface waters ($n = 8$, $p = 0.18$) and −0.290 for wells and the spring ($n = 6$, $p = 0.58$), and −0.484 when Lake Karakol was represented by a single point ($n = 12$, $p = 0.11$). The salinity-related associations also depend on the contrast between the two regimes: among the surface waters, ρ was only 0.05 for Cl^- and TDS ($n = 8$), whereas among the wells and the spring it was 0.81 for Cl^- and $Na^+ + K^+$ ($n = 6$; not significant after FDR correction). With Lake Karakol represented by a single point, the associations with Cl^-, $Na^+ + K^+$ and TDS remained significant (FDR-adjusted $p_{perm} = 0.036$–0.045), and in the leave-one-out analysis ρ ranged from 0.66 to 0.79 for Cl^- and from 0.62 to 0.74 for TDS. When the five May samples with indicative Li^+ results (IDs 1, 2, 3, 7 and 14) were excluded ($n = 9$), ρ was 0.586 for TDS (permutation $p = 0.105$; FDR-adjusted $p = 0.349$), 0.695 for Cl^-, 0.678 for $Na^+ + K^+$ (FDR-adjusted permutation $p = 0.259$ for both) and 0.427 for SO_4^{2-}, and none of the ten associations remained significant after FDR

correction. Given the reduced sample size, this does not demonstrate the absence of an association, but it shows that the significance of the pooled associations depends on the samples whose Li^+ results are indicative.

The relationships between Li^+ and the major cations Ca^{2+}, Mg^{2+}, and $Na^+ + K^+$ are illustrated in Figure 7. Considerable scatter remained among the samples, indicating that variation in individual major-ion concentrations alone does not fully explain Li distribution.

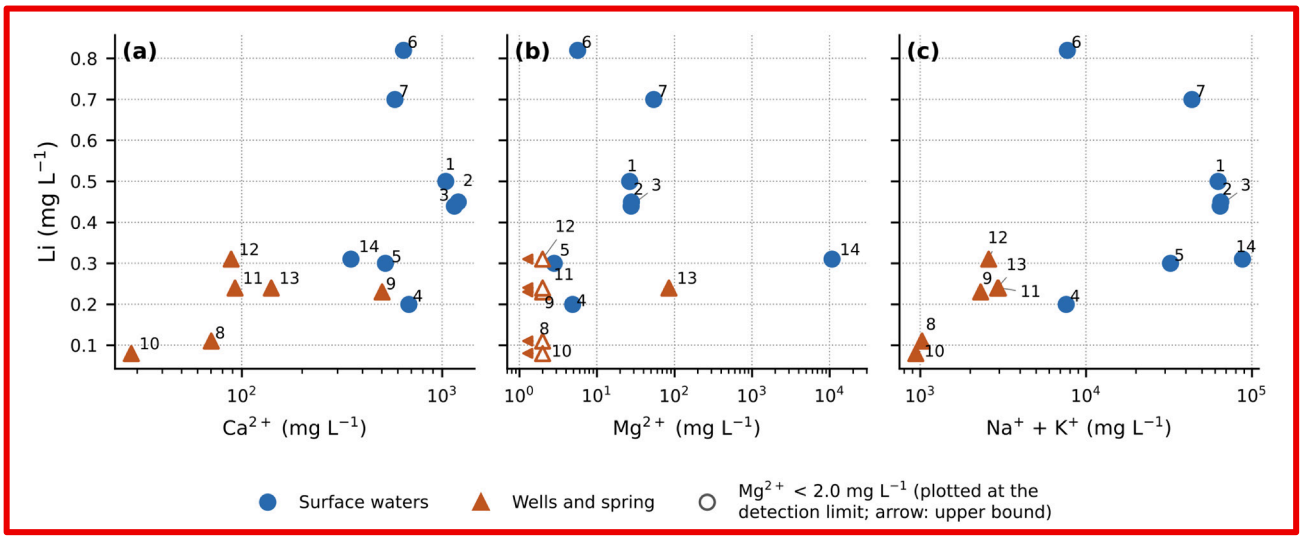


Figure 7. Relationships between Li^+ concentration and major cations in May 2026: (**a**) Ca^{2+}, (**b**) Mg^{2+}, and (**c**) $Na^+ + K^+$. Major-cation concentrations are shown on logarithmic scales; point labels are site IDs (Table 1). Open triangles: Mg^{2+} below the 2.0 mg L^{-1} detection limit, plotted at the detection limit; arrows indicate that the true value is lower. Circles: surface waters; triangles: wells and the spring. Li^+ values of IDs 1, 2, 3, 7 and 14 are indicative (Section 3.3).

4.4. Ion-to-Lithium Ratios of the May Samples

Selected hydrochemical indicators were used to compare the ionic matrix of the investigated waters in relation to Li occurrence. Particular attention was given to Mg/Li and Ca/Li mass ratios, because Mg^{2+} and Ca^{2+} are major competing ions in Li-bearing aqueous systems and can strongly influence the selectivity and efficiency of lithium separation [33–36].

Among the May samples, Ashysor Lower (ID 6) combined the highest Li^+ concentration (0.82 mg L^{-1}) with an Mg/Li mass ratio of about 7; however, this ratio is based on a Mg^{2+} concentration (≈5.7 mg L^{-1}) below the range of application of the titrimetric method and is therefore semi-quantitative. The same water had a Ca/Li ratio of about 780 and a total hardness of 32.47 meq L^{-1}. Ashysor (ID 7) contained 0.70 mg L^{-1} Li^+ with an Mg/Li ratio of 77.5.

Kishi Oymasha (ID 14) represented the most contrasting matrix, with an Mg/Li mass ratio of about 3.5×10^4. For Sad Dubsky F-1 (ID 12) and Kuryk (ID 11), the Mg^{2+} concentrations implied by the originally reported ratios (≈0.20 mg L^{-1}) are below the 2.0 mg L^{-1} detection limit of the method; they are now reported as censored values, so that only upper bounds can be given (Mg/Li < 6.5 and <8.3, respectively).

The principal hydrochemical parameters and ion-to-Li mass ratios used for preliminary comparison of the selected waters are summarized in Table 3 for all 14 first-campaign samples; the values for both dates are given in the Supplementary Materials.

Figure 8 shows Li^+ concentration against the Mg/Li mass ratio for the May samples. Because Li appears both on the vertical axis and in the denominator of Mg/Li, an inverse pattern is expected partly by construction; the figure is therefore descriptive and is not used as evidence of a geochemical trade-off.

Table 3. Hydrochemical indicators and ion/Li mass ratios of the first-campaign samples (May 2026, $n = 14$).

Site ID	Sampling Site	Li^+ (mg L^{-1})	TDS (g L^{-1})	Hardness (meq L^{-1})	pH	T (°C)	Mg/Li	Ca/Li	$10^5 \times$ Li/Cl
1	Karakol No. 1	0.50	168.04	54.18	8.0	12.4	53.0	2.08×10^3	0.53
2	Karakol No. 2	0.45	175.07	62.30	7.9	11.8	62.0	2.67×10^3	0.46
3	Karakol No. 3	0.44	173.25	59.78	7.9	11.5	63.0	2.62×10^3	0.45
4	Ashyagar, upper reach	0.20	23.30	34.41	7.4	10.0	24.3 [b]	3.41×10^3	1.75
5	Ashyagar, lower reach	0.30	82.00	26.23	7.4	9.5	9.3 [b]	1.74×10^3	0.65
6	Ashysor Lower	0.82	23.95	32.47	7.6	12.0	6.95 [b]	782	7.00
7	Ashysor	0.70	137.55	32.46	7.4	12.0	77.5	802	1.10
8	Ashyagar–Alatobe	0.11	2.93	3.50	7.4	40.0	<18.2 [a]	638	9.39
9	Northern Karagiye	0.23	8.19	25.00	7.3	27.4	<8.7 [a]	2.18×10^3	7.04
10	14th Siding	0.08	2.89	14.00	7.5	40.2	<25.0 [a]	3.51×10^3	8.67
11	Kuryk (Eralievo F-1)	0.24	8.08	4.60	7.3	25.1	<8.3 [a]	384	7.95
12	Sad Dubsky F-1	0.31	6.78	4.40	7.4	31.0	<6.5 [a]	285	8.91
13	Radon Spring	0.24	8.52	14.01	6.6	41.2	354.6	585	5.88
14	Kishi Oymasha	0.31	274.98	900.73	7.6	13.4	3.46×10^4	1.13×10^3	0.22

Ratios are mass ratios. TDS is the sum of the measured ions; hardness is calculated from Ca^{2+} and Mg^{2+} (Section 3.2). [a] Mg^{2+} below the 2.0 mg L^{-1} detection limit of GOST 26449.1-85 [29]; the value is an upper bound. [b] Semi-quantitative: Mg^{2+} (2.8–5.7 mg L^{-1}) is below the 20 mg L^{-1} range of application of the method. Li^+ values of IDs 1, 2, 3, 7 and 14 are indicative (TDS > 100 g L^{-1}; Section 3.3).

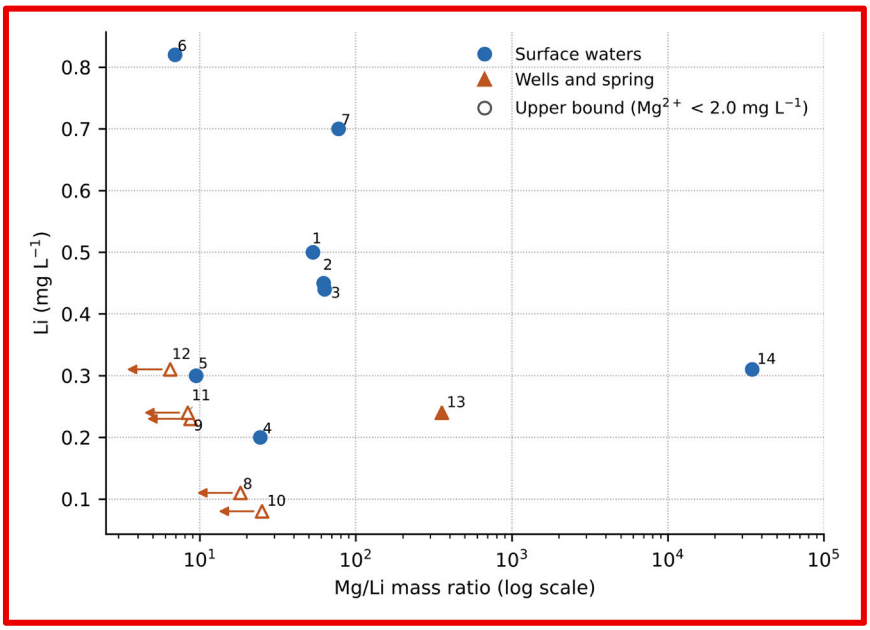


Figure 8. Li^+ concentration versus Mg/Li mass ratio in May 2026 (descriptive plot; Li appears on both axes). The Mg/Li axis is logarithmic; point labels are site IDs (Table 1). Open triangles with arrows: upper bounds ($Mg^{2+} < 2.0$ mg L^{-1}). Circles: surface waters; triangles: wells and the spring. Li^+ values of IDs 1, 2, 3, 7 and 14 are indicative (Section 3.3).

The ratios show that waters with similar Li^+ concentrations can differ by several orders of magnitude in Mg/Li and Ca/Li. They are reported as descriptive indicators for selecting samples for confirmatory analysis and do not constitute evidence of technical or economic feasibility.

5. Discussion

5.1. Hydrogeochemical Associations and Possible Controls on Li Distribution

The results show that Li distribution in the investigated waters is not explained by salinity alone. The clearest example is the contrast between Kishi Oymasha (ID 14) and

Ashysor Lower (ID 6) described in Section 4.3, which shows that a single proportional Li–TDS relationship does not describe all waters. This contrast is consistent with several explanations that the present data cannot discriminate: Kishi Oymasha may derive its salinity mainly from Li-poor salts, may have lost Li to secondary minerals during brine evolution, or may differ in source water from Ashysor Lower. Because the Li^+ result of Kishi Oymasha is indicative (Section 3.3), this contrast is not used as definitive quantitative evidence of the relationship between Li^+ and salinity.

The statistically significant positive associations of Li^+ with Cl^-, $Na^+ + K^+$, SO_4^{2-}, and TDS in May, which remained significant after permutation-based FDR correction, are consistent with Li^+ concentrations increasing together with other dissolved constituents as salinity increases. In contrast, the positive associations with Ca^{2+}, Mg^{2+}, and total hardness did not remain statistically significant after permutation-based FDR correction (Table 2). Because the major-ion concentrations and calculated TDS are closely interrelated, the significant associations represent a common salinity-related pattern rather than independent evidence of specific geochemical processes. Moreover, the pooled correlations combine surface waters and groundwater systems that differ systematically in temperature and hydrological setting (Section 4.3). These associations were also not robust to the exclusion of the five May samples with indicative Li^+ results (Section 4.3).

To test whether the Li–TDS association depended on the most mineralized and analytically challenging sample, a leave-one-out sensitivity analysis excluded Kishi Oymasha (ID 14) from the first-campaign dataset. Spearman's rank correlation between Li^+ and calculated TDS was $\rho = 0.696$ ($n = 14$; asymptotic two-sided $p = 0.00569$) for the complete dataset and $\rho = 0.737$ ($n = 13$; asymptotic two-sided $p = 0.00403$) after exclusion. Two-sided Monte Carlo permutation tests (19,999 resamples; random seed 2026) yielded $p = 0.0063$ and $p = 0.0058$, respectively. Thus, the positive pooled Li–TDS rank association was not driven solely by Kishi Oymasha. These are unadjusted p-values for this targeted sensitivity analysis; they are not replacements for the FDR-adjusted results in Table 2. Because of the small, hydrochemically heterogeneous sample, the association should not be interpreted as causal. Excluding a potentially matrix-affected observation tests the statistical robustness of the association but does not validate the Li measurements in the remaining saline samples. When all five May samples with indicative Li^+ results (IDs 1, 2, 3, 7 and 14) were excluded, the Li–TDS association weakened to $\rho = 0.586$ ($n = 9$; permutation $p = 0.105$), and none of the ten associations remained significant after FDR correction (Section 4.3). Given the reduced sample size, this does not demonstrate the absence of an association, but it qualifies the robustness of the pooled associations.

We therefore regard evaporative concentration, differences in Li supply, mixing between waters of different origin, and water–rock interaction as competing or complementary hypotheses. Similar multi-process controls have been reported in other Li-bearing systems, where enrichment depends not only on aridity and evaporation but also on solute supply from groundwater, springs, weathering, or deeper fluids [7–11], and deep-brine studies emphasize lithological sources, mineral dissolution, ion exchange, and prolonged water–rock interaction [13,37,38]. A first test of the simple evaporation hypothesis is provided by the Li/Cl ratio, which remains constant if a water is concentrated or diluted without gain or loss of Li and Cl: in the first campaign, Li/Cl was highest in the wells and the spring ($5.9–9.4 \times 10^{-5}$; TDS 2.9–8.5 g L^{-1}) and in Ashysor Lower (7.0×10^{-5}), and lowest in the most saline waters, Lake Karakol ($4.5–5.3 \times 10^{-6}$; TDS 168–175 g L^{-1}) and Kishi Oymasha (2.2×10^{-6}; TDS 275 g L^{-1}) (Table 3). Li/Cl therefore decreases by more than an order of magnitude as TDS increases, so the most saline waters are not simply evaporated equivalents of the less saline ones; their composition requires a Cl^- source with low Li/Cl (e.g., seawater or halite dissolution), Li removal, or different source waters. Discriminating

among the remaining hypotheses at individual sites requires site-specific hydrological data and independent tracers such as Li and water stable isotopes (Section 5.5).

Thus, the dataset is consistent with the view that salinity records hydrochemical evolution, whereas Li^+ concentration additionally depends on Li supply; this interpretation remains a hypothesis to be tested.

5.2. Differences Between the May and August Sampling Dates

At the eight resampled sites, Li^+ was higher in August than in May at seven sites (Section 4.2). These are differences between two sampling dates in one year; they do not establish a recurring seasonal cycle and cannot distinguish seasonal behaviour from short-term events. Moreover, the resampled sites are not a random subset of the network, because five surface-water sites had dried out and one well was inaccessible.

The climatic context helps to frame these differences (Section 2). The first campaign took place in May, when the surface waters were 9.5–13.4 °C. The following months were wetter than average (51 mm of precipitation from June to August 2026 versus a 1991–2020 mean of 30 mm), but evaporative demand (590 mm ET_0) still greatly exceeded precipitation, and summer air temperatures were close to normal. The paired data of the three resampled surface waters do not show a uniform pattern (Supplementary Materials). In the lower Ashyagar reach, Cl^- increased by 83% and Li^+ by 663%; at Ashysor Lower, both decreased (Cl^- by 18% and Li^+ by 4%); and at Karakol No. 1, Cl^- decreased by 93% (from 94,430 to 6923 mg L^{-1}) while Li^+ changed little (+9%) (Section 3.1). At all three sites, however, Li/Cl was higher in August than in May, i.e., Li^+ increased relative to Cl^-, which simple evaporative concentration or dilution cannot produce. In the four wells and the spring, Li^+ increased by 72–376% while Cl^- changed by only −4% to +17% and temperature by −0.7 to +2.5 °C, so Li/Cl also increased at all five groundwater sites. For these sites, possible explanations include changes in pumping or discharge regime that draw water from different parts of the aquifer, mixing with a more Li-rich component, and a systematic difference between the two analytical sequences; the last cannot be excluded because matrix-spike validation was not performed (Section 3.3). The operating regime of the wells between the two campaigns is not known, and QC results were not reported separately for the two analytical sequences. The pooled May correlation between Li^+ and temperature cannot be used to evaluate within-site temperature effects.

The drying of five surface-water sites by August shows that the surface-water network contracts strongly in summer even in a year with near-normal summer climate. Such changes can modify water volume, hydraulic connectivity, and the relative contribution of groundwater and surface-water inputs, and thereby both salinity and Li^+ concentration.

The 2.29 mg L^{-1} Li^+ concentration measured in the lower Ashyagar reach slightly exceeds the maximum found in our previous study of formation waters from the Karazhanbas, Zhetybay and Uzen oil fields (1.85 mg L^{-1}) [15]. A preliminary explanation is evaporative concentration of residual water in the lower reach of an intermittent river after the end of spring runoff, possibly combined with inflow of more mineralized groundwater along the valley. Whether Li^+ increased in proportion to Cl^- (evaporation) or more than Cl^- (additional Li supply) can be tested with the paired Li/Cl ratio. Between the two campaigns, Cl^- increased from 46,150 to 84,313 mg L^{-1} (×1.8), whereas Li^+ increased from 0.30 to 2.29 mg L^{-1} (×7.6), so that the Li/Cl mass ratio rose about fourfold, from 6.5×10^{-6} to 2.7×10^{-5}. Evaporative concentration alone therefore does not account for the increase, which points to an additional Li supply or a change in the water feeding the lower reach. The water temperature at this site increased from 9.5 °C in May to 23.1 °C in August; however, comparable increases at the other two resampled surface waters (Karakol No. 1, from 12.4 to 22.4 °C; Ashysor Lower, from 12.0 to 21.2 °C) suggest that seasonal warming likely

contributed substantially to the observed temperature increase. The available observations do not allow the relative contributions of seasonal warming and groundwater inflow to be quantified. A contribution of warm, Li^+-bearing water from a deep source, whose proportion would increase as surface flow declines and which would raise both temperature and Li^+, is therefore possible but cannot be confirmed with the present data; discharge measurements and isotopic tracers would be required to test it. Because this value is based on a single sample, analytical confirmation and repeated field sampling are required before it is regarded as persistent.

These observations suggest that a single survey may not represent Li^+ concentrations in dynamic surface-water systems. Sampling at least every three to four months over several years would be required to separate recurring seasonal variation from interannual and event-scale variability.

5.3. Comparison with Other Lithium-Bearing Water Systems

Compared with mature salt-lake brines and deep sedimentary-basin brines, the investigated Mangystau waters contain low to moderate Li^+ concentrations (0.08–2.29 mg L^{-1}). A comparison with representative Li-bearing aqueous systems is provided in Table 4. The comparison systems were selected because they (i) represent the main types of Li-bearing aqueous systems—salt-lake brines with their recharge waters, and deep sedimentary-basin brines—and (ii) report both Li^+ concentrations and a hydrochemical interpretation of Li sources; regional datasets from Kazakhstan [14,15] were added for context.

Table 4. Comparison of lithium concentrations and principal hydrogeochemical characteristics of the present study with selected Li-bearing aqueous systems reported in the literature.

Region/Study	Water System	Reported Li^+ (mg L^{-1})	Main Interpretation
Present study, Mangystau	Lakes, salt-flat, rivers, wells, and spring	0.08–0.82 (May); 0.25–2.29 (August)	Salinity alone does not explain Li; controls unresolved
Qinghai–Tibetan Plateau [8]	Li-rich salt lakes	23–2895	Li source, aridity, closed-basin evolution, and prolonged residence
Western Kunlun [9]	Rivers, springs, and salt lake	0.01–287.86	Li-rich springs and fluid pathways; evaporation and mixing
Lakko Co, Tibet [38]	Recharge waters and salt-lake brine	0.11–590.8	Rock weathering, hot-spring input, and water–rock interaction
Jianghan Basin [37]	Deep brines	up to 97.85	Evaporation, halite dissolution, and water–rock interaction
Shu–Sarysu, Kazakhstan [14]	Deep formation brines	24.46–55.11	Water–rock interaction, evaporative concentration, and diagenetic brine evolution
Mangystau formation waters [15]	Oilfield formation waters	0.30–1.85	Reservoir hydrochemical evolution; salinity is not the sole control on Li

Ranges are given as reported in the cited studies; depending on the study, they refer to individual samples or to summary values and to different water components, and they are shown for orientation only.

Li^+ concentrations reported for salt-lake and deep-basin brines exceed the highest value measured here (2.29 mg L^{-1}) by up to three orders of magnitude (Table 4). The cited studies attribute these concentrations to Li-rich source material, arid closed-basin hydrology, and prolonged brine evolution on the Qinghai–Tibetan Plateau [8]; to Li-rich springs combined with evaporation and mixing in the western Kunlun Mountains [9]; to rock weathering, hot-spring input, and water–rock interaction at Lakko Co [38]; and to

evaporation, halite dissolution, and water–rock interaction in deep brines of the Jianghan Basin [37].

By contrast, previously studied Mangystau oilfield formation waters contained 0.30–1.85 mg L^{-1} Li^+ [15], a range that overlaps considerably with the present natural-water dataset. The maximum concentration observed in this study, 2.29 mg L^{-1} in the lower Ashyagar reach, slightly exceeded the previously reported maximum for regional formation waters. This overlap in concentration range does not establish a common source, residence time, or recovery potential.

Overall, the investigated Mangystau waters are not comparable to highly evolved Li-rich brines in terms of absolute Li^+ concentration. The highest values are site-specific and warrant targeted monitoring, source-tracing studies, and further hydrochemical evaluation.

5.4. Preliminary Considerations for Recovery-Oriented Testing

Li^+ concentration alone is insufficient for a preliminary evaluation of recovery potential. The ionic matrix—particularly Mg^{2+}, Ca^{2+}, Mg/Li, Ca/Li, TDS, hardness, and pH—is equally important, because these parameters affect pretreatment requirements and selective Li separation [33–36]. Moreover, the Li^+ concentrations measured here ($\leq$2.29 mg L^{-1}) are far below those of the salt-lake and subsurface brines considered in reviews of Li extraction technologies [33–36].

No sample can currently be ranked as the most favourable. Ashysor Lower (ID 6) combines the highest May Li^+ concentration (0.82 mg L^{-1}) with a low but semi-quantitative Mg/Li ratio ($\approx$7), yet its Ca/Li ratio ($\approx$780) and hardness (32.47 meq L^{-1}) indicate a Ca-dominated matrix, and Ca^{2+} is also a competing ion for several separation approaches [33–36]. The low Mg/Li ratios originally reported for Sad Dubsky F-1 and Kuryk are upper bounds only (Section 4.4). The lower Ashyagar reach, which yielded the highest Li^+ concentration (2.29 mg L^{-1} in August), lacks a complete characterization of its August matrix, because the August Na^+ result failed the charge-balance check (Section 3.2).

Kishi Oymasha (ID 14), with very high TDS and an Mg/Li ratio of about 3.5×10^4, represents the most complex matrix among the samples. Sad Dubsky F-1 and Kuryk had low hardness (4.40 and 4.60 meq L^{-1}) but also low Li^+ concentrations (0.31 and 0.24 mg L^{-1}).

Accordingly, any selection of waters for laboratory tests should consider Li abundance, the full competing-ion composition (Mg^{2+}, Ca^{2+}, Na^+, K^+), salinity, water availability, and temporal variability together, rather than a single ratio.

The present assessment should therefore be regarded strictly as preliminary hydrochemical screening. Direct recovery experiments are required to evaluate selectivity, recovery efficiency, pretreatment demand, reagent consumption, energy requirements, and overall technical feasibility. The immediate next step is confirmatory sampling of Ashysor Lower and the lower Ashyagar reach with complete matrix characterization, rather than recovery testing.

5.5. Study Limitations and Future Research

Several limitations affect interpretation of the present results. First, only 14 sites were investigated, and only eight sites were sampled during both campaigns. The dataset therefore captures two sampling dates rather than a complete annual hydrochemical cycle, and the August subset is biased towards groundwater sites.

Second, the study combines hydrologically distinct water types, including saline lakes, salt-flat, rivers, groundwater wells, and a spring. This heterogeneity is useful for regional comparison but limits causal interpretation of pooled statistical relationships. The observed correlations should therefore be interpreted as hydrochemical associations rather than direct evidence of individual geochemical processes. In addition, the three Karakol points

belong to one managed water body and may not be independent. The Karakol samples were collected at a depth of 0.4 m below the water surface. Although the lake was reported to be shallow (generally less than 1 m deep), vertical profiles of temperature and electrical conductivity were not measured. Therefore, persistent thermal or chemical stratification cannot be conclusively excluded. The analytical results characterize the sampled depth and should not be assumed to represent the entire water column.

Third, the inferred roles of evaporation, groundwater contribution, mixing, and water–rock interaction were not independently quantified with isotopic or mineralogical tracers. Isotopic analyses were not performed because the authors had no access to a laboratory performing Li-isotope or water-isotope analyses. Lithium isotopes would be particularly informative, because evaporative concentration does not appreciably fractionate Li isotopes, whereas uptake of Li into secondary minerals during water–rock interaction preferentially removes ^{6}Li [6,9,10,38]; stable water isotopes, host-rock characterization, and groundwater-flow tracers would further constrain Li sources and mixing.

Fourth, the 2.29 mg L^{-1} value recorded in the lower Ashyagar reach represents a single observation and requires confirmation by repeated monitoring. Specifically, removing Kishi Oymasha from the first-campaign correlation analysis did not eliminate the positive Li–TDS association (Section 5.1), whereas excluding all five May samples with indicative Li^{+} results removed the statistical significance of all associations (Section 4.3); neither sensitivity result resolves the potential ICP-OES matrix bias or replaces matrix-specific experimental validation.

Fifth, matrix-spike or standard-addition validation of Li in the most saline samples was not performed, low Mg^{2+} concentrations are partly below the detection limit of the titrimetric method, first-campaign Na^{+} and K^{+} are available only as their sum, the August Na^{+} data failed the charge-balance check, and well-construction data and purging records were not available. These limitations mainly affect the hypersaline samples, the Mg-based ratios, and the interpretation of the groundwater sites.

Finally, no direct Li-recovery experiments were conducted. The hydrochemical screening therefore identifies potentially interesting waters but does not establish technological or economic feasibility.

Future work should focus on repeated sampling at least every three to four months over several years, expanded spatial coverage, isotopic source tracing, mineralogical characterization, and targeted extraction experiments. Together, these approaches would allow the relative contributions of Li-source availability, water–rock interaction, hydrological transport, mixing, and evaporation to be tested more rigorously.

6. Conclusions

Dissolved Li^{+} in contrasting waters of the Mangystau Region ranged from 0.08 to 0.82 mg L^{-1} in May 2026 (14 sites) and from 0.25 to 2.29 mg L^{-1} in August 2026 at the eight sites that could be resampled, and Li^{+} was higher in August at seven of these eight sites. These are differences between two sampling dates and do not by themselves establish a seasonal cycle.

High salinity does not necessarily correspond to high Li^{+} concentrations: the most saline water, Kishi Oymasha (TDS ≈ 275 g L^{-1}), contained only 0.31 mg L^{-1} Li^{+}, an indicative value. In May, significant positive associations with Li^{+} remained for Cl^{-}, Na^{+} + K^{+}, SO_4^{2-}, and TDS after permutation-based FDR correction. These associations depend on the five most saline May samples, whose Li^{+} results are indicative because matrix-specific validation was not performed; without them (n = 9), none remained significant after FDR correction. Although positive correlations were also observed for Ca^{2+}, Mg^{2+}, and total hardness, these associations were not statistically significant after this correction.

The observed salinity-related relationships do not identify the contributions of individual hydrogeochemical processes.

Ion/Li ratios differ by several orders of magnitude among waters with similar Li^+ concentrations, so Li^+ concentration alone is not a sufficient criterion for selecting waters for further study. None of the samples can yet be ranked for Li recovery; confirmatory sampling with complete matrix characterization is required first, particularly for Ashysor Lower and the lower Ashyagar reach.

Overall, the study provides a preliminary regional hydrochemical baseline for Li in the natural and near-natural waters of Mangystau. Evaporative concentration, differences in Li supply, mixing, and water–rock interaction remain competing or complementary hypotheses; testing them will require repeated sampling over at least a full year, site-specific hydrological data, and isotopic tracers.

Supplementary Materials: The following supporting information can be downloaded at: https://www.mdpi.com/article/10.3390/geosciences16110457/s1, Table S1, hydrochemical and lithium data for the May and August 2026 sampling campaigns, including sampling-site coordinates, physicochemical parameters, and major-ion concentrations; Table S2, lithium concentrations and dilution factors used for ICP-OES analysis; and Script S1 (Python), providing reproducible hydrochemical calculations and statistical analyses.

Author Contributions: Conceptualization, A.B., A.S., A.T. and R.S.; methodology, A.B., A.T., Y.A. and S.M.; software, R.S.; validation, K.K., A.S. and S.M.; formal analysis and investigation, A.B., A.T., Y.A., R.S. and A.S.; resources, K.K.; data curation, A.B., S.M. and A.S.; writing—original draft preparation, A.B., R.S. and A.T.; writing—review and editing: A.S., K.K., Y.A. and S.M.; visualization, K.K.; supervision, A.S.; project administration, A.B.; funding acquisition, A.B. All authors have read and agreed to the published version of the manuscript.

Funding: This research was financially supported by the Science Committee of the Ministry of Science and Higher Education of the Republic of Kazakhstan, Grant No. AP22686075, "Investigation of the ion-salt composition of lithium-containing natural and wastewater of the Mangystau region and identification of industrial lithium sources".

Data Availability Statement: The data supporting the findings of this study are provided in the article (Tables 1–4) and the accompanying Supplementary Materials (Tables S1 and S2). The Supplementary Materials also include a Python analysis script (Script S1), together with the corresponding input datasets, to facilitate independent reproduction and verification of the hydrochemical calculations and statistical analyses.

Acknowledgments: Climate data were obtained from the ERA5 reanalysis through the Open-Meteo Historical Weather API.

Conflicts of Interest: Authors Azamat Tarbanov and Yerbolat Ayapbergenov were employed by Branch of Limited Liability Partnership "KazMunaiGas Engineering" "KazNIPImunaigas". The remaining authors declare that the research was conducted in the absence of any commercial or financial relationships that could be construed as a potential conflict of interest.

References

1. Flexer, V.; Baspineiro, C.F.; Galli, C.I. Lithium recovery from brines: A vital raw material for green energies with a potential environmental impact in its mining and processing. *Sci. Total Environ.* **2018**, *639*, 1188–1204. [CrossRef] [PubMed]
2. Vera, M.L.; Torres, W.R.; Galli, C.I.; Chagnes, A.; Flexer, V. Environmental impact of direct lithium extraction from brines. *Nat. Rev. Earth Environ.* **2023**, *4*, 149–165. [CrossRef]
3. Balaram, V.; Santosh, M.; Satyanarayanan, M.; Srinivas, N.; Gupta, H. Lithium: A review of applications, occurrence, exploration, extraction, recycling, analysis, and environmental impact. *Geosci. Front.* **2024**, *15*, 101868. [CrossRef]
4. Adeel, M.; Zain, M.; Shakoor, N.; Ahmad, M.A.; Azeem, I.; Aziz, M.A.; Tulcan, R.X.S.; Rathore, A.; Tahir, M.; Horton, R.; et al. Global navigation of lithium in water bodies and emerging human health crisis. *npj Clean Water* **2023**, *6*, 33. [CrossRef]

5. Lindsey, B.D.; Belitz, K.; Cravotta, C.A.; Toccalino, P.L.; Dubrovsky, N.M. Lithium in groundwater used for drinking-water supply in the United States. *Sci. Total Environ.* **2021**, *767*, 144691. [CrossRef] [PubMed]
6. Ji, T.-T.; Jiang, X.-W.; Gou, L.-F.; Jin, Z.; Zhang, H.; Wan, L.; Han, G.; Guo, H.; Wang, X.-S. Behaviors of lithium and its isotopes in groundwater with different concentrations of dissolved CO_2. *Geochim. Cosmochim. Acta* **2022**, *326*, 313–327. [CrossRef]
7. Munk, L.A.; Boutt, D.F.; Hynek, S.A.; Moran, B.J. Hydrogeochemical fluxes and processes contributing to the formation of lithium-enriched brines in a hyper-arid continental basin. *Chem. Geol.* **2018**, *493*, 37–57. [CrossRef]
8. Li, Q.; Fan, Q.; Wang, J.; Qin, Z.; Zhang, X.; Wei, H.; Du, Y.; Shan, F. Hydrochemistry, distribution and formation of lithium-rich brines in salt lakes on the Qinghai–Tibetan Plateau. *Minerals* **2019**, *9*, 528. [CrossRef]
9. Li, Y.-L.; Miao, W.-L.; He, M.-Y.; Li, C.-Z.; Gu, H.-E.; Zhang, X.-Y. Origin of lithium-rich salt lakes on the western Kunlun Mountains of the Tibetan Plateau: Evidence from hydrogeochemistry and lithium isotopes. *Ore Geol. Rev.* **2023**, *155*, 105356. [CrossRef]
10. Xue, F.; Tan, H.; Zhang, X.; Santosh, M.; Cong, P.; Ge, L.; Li, C.; Chen, G.; Zhang, Y. Contrasting sources and enrichment mechanisms in lithium-rich salt lakes: A Li-H-O isotopic and geochemical study from northern Tibetan Plateau. *Geosci. Front.* **2024**, *15*, 101768. [CrossRef]
11. Zhou, J.; Li, B.; He, M.; Jiao, J.; Tang, Z.; Li, Z. Hydrochemical characteristics and sources of lithium in carbonate-type salt lake in Tibet. *Sustainability* **2023**, *15*, 16235. [CrossRef]
12. Chelnokov, G.; Lavrushin, V.; Bragin, I.; Abdullaev, A.; Aidarkozhina, A.; Kharitonova, N. Geochemistry of thermal and cold mineral water and gases of the Tien Shan and the Pamir. *Water* **2022**, *14*, 838. [CrossRef]
13. Absametov, M.; Chensizbayev, D.; Itemen, N.; Murtazin, E.; Mirlas, V.; Zilberbrand, M.; Anker, Y. Origin of lithium-rich deep formation waters in Upper Devonian–Lower Carboniferous sediments of Shu-Sarysu gas fields, Kazakhstan, studied by hydrochemical modeling. *Groundw. Sustain. Dev.* **2025**, *30*, 101500. [CrossRef]
14. Tazhiyev, S.; Murtazin, Y.; Adenova, D.; Toktar, A.; Rakhmetov, I.; Abdizhalel, M.; Akylbayeva, A.; Yerezhep, D. Hydrogeochemistry of lithium-bearing brines of the Shu–Sarysu Sedimentary Basin. *Water* **2026**, *18*, 1774. [CrossRef]
15. Boranbayeva, A.; Serikbayeva, A. Hydrogeochemical assessment of lithium in oilfield formation waters of the Mangystau Region, Kazakhstan: Distribution, geochemical controls, and preliminary resource evaluation. *ChemEngineering* **2026**, *10*, 88. [CrossRef]
16. Kozhagulova, A.; Dillinger, A.; Bayramov, E.; Iltukov, R.; Holbrook, J.; Fustic, M. Geothermal energy potential of the Mangyshlak Basin, western Kazakhstan: A preliminary assessment based on stratigraphy and temperature data. *Geothermics* **2023**, *109*, 102655. [CrossRef]
17. Ni, J.; Zhao, D.; Liao, X.; Li, X.; Fu, L.; Chen, R.; Xia, Z.; Liu, Y. Sedimentary architecture analysis of deltaic sand bodies using sequence stratigraphy and seismic sedimentology: A case study of Jurassic deposits in Zhetybay Oilfield, Mangeshrak Basin, Kazakhstan. *Energies* **2022**, *15*, 5306. [CrossRef]
18. Chakabaev, S.E.; Kononov, Y.S.; Votsalevsky, E.S.; Ivanov, V.A.; Shakhovoy, A.I. *Geology and Oil and Gas Potential of South Mangyshlak*; Nauka: Alma-Ata, Kazakhstan, 1967; 227p. (In Russian)
19. Hersbach, H.; Bell, B.; Berrisford, P.; Hirahara, S.; Horányi, A.; Muñoz-Sabater, J.; Nicolas, J.; Peubey, C.; Radu, R.; Schepers, D.; et al. The ERA5 global reanalysis. *Q. J. R. Meteorol. Soc.* **2020**, *146*, 1999–2049. [CrossRef]
20. Open-Meteo. Historical Weather API. Available online: https://open-meteo.com/en/docs/historical-weather-api (accessed on 22 October 2026).
21. Allen, R.G.; Pereira, L.S.; Raes, D.; Smith, M. Crop Evapotranspiration—Guidelines for Computing Crop Water Requirements. In *FAO Irrigation and Drainage Paper 56*; FAO: Rome, Italy, 1998.
22. U.S. Geological Survey. Chapter A4. Collection of Water Samples, ver. 2.0. In *National Field Manual for the Collection of Water-Quality Data*; Techniques of Water-Resources Investigations, Book 9, Chapter A4; U.S. Geological Survey: Reston, VA, USA, 2006; 166p. [CrossRef]
23. Dąbrowska, D.; Witkowski, A.J.; Sołtysiak, M. Representativeness of the groundwater monitoring results in the context of its methodology: Case study of a municipal landfill complex in Poland. *Environ. Earth Sci.* **2018**, *77*, 266. [CrossRef]
24. Key Biodiversity Areas Partnership. Karakol Lake (KBA 20927). Available online: https://www.keybiodiversityareas.org/site/factsheet/20927 (accessed on 22 October 2026).
25. Tengrinews. Pink Flamingos and Swans Fly Here: Lake Karakol, Which Made the Whole World Fall in Love with It. Available online: https://tengrinews.kz/my-country/syuda-priletayut-rozovyie-flamingo-lebedi-ozero-karakol-425739/ (accessed on 22 October 2026).
26. *ISO 5667-3:2024*; Water Quality—Sampling—Part 3: Preservation and Handling of Water Samples, 6th ed. ISO: Geneva, Switzerland, 2024.
27. U.S. Environmental Protection Agency. *Method 200.7: Determination of Metals and Trace Elements in Water and Wastes by Inductively Coupled Plasma—Atomic Emission Spectrometry, Revision 4.4*; U.S. Environmental Protection Agency: Cincinnati, OH, USA, 1994.
28. Rakhimov, T.; Tazhiyev, S.; Rakhimova, V.; Smolyar, V.; Toktar, A.; Akylbayeva, A.; Abdizhalel, M.; Yerezhep, D. Groundwater quality, contamination, and resource potential for pasture livestock watering in arid western Kazakhstan. *Water* **2026**, *18*, 1258. [CrossRef]

29. *GOST 26449.1-85*; Stationary Distillation Desalination Plants. Methods of Chemical Analysis of Saline Waters. Izdatel'stvo Standartov: Moscow, Russia, 1985. (In Russian)
30. Hach Company. *Sulfate, SulfaVer 4 Method 8051, Powder Pillows, DOC316.53.01135*, 11th ed.; Hach Company: Loveland, CO, USA, 2019.
31. Benjamini, Y.; Hochberg, Y. Controlling the false discovery rate: A practical and powerful approach to multiple testing. *J. R. Stat. Soc. Ser. B* **1995**, *57*, 289–300. [CrossRef]
32. Sulin, V.A. *Waters of Petroleum Deposits in the System of Natural Waters*; Gostoptekhizdat: Moscow, Russia; Leningrad, Russia, 1946. (In Russian)
33. Mojid, M.R.; Lee, K.J.; You, J. A review on advances in direct lithium extraction from continental brines: Ion-sieve adsorption and electrochemical methods for varied Mg/Li ratios. *Sustain. Mater. Technol.* **2024**, *40*, e00923. [CrossRef]
34. Liu, G.; Zhao, Z.; Ghahreman, A. Novel approaches for lithium extraction from salt-lake brines: A review. *Hydrometallurgy* **2019**, *187*, 81–100. [CrossRef]
35. Zhang, Y.; Hu, Y.; Wang, L.; Sun, W. Systematic review of lithium extraction from salt-lake brines via precipitation approaches. *Miner. Eng.* **2019**, *139*, 105868. [CrossRef]
36. Disu, B.; Rafati, R.; Sharifi Haddad, A.; Mendoza Roca, J.A.; Iborra Clar, M.I.; Soleymani Eil Bakhtiari, S. Review of recent advances in lithium extraction from subsurface brines. *Geoenergy Sci. Eng.* **2024**, *241*, 213189. [CrossRef]
37. Yan, K.; Wang, C.; Chen, R.; Liu, C.; Wang, J.; Yu, X.; Shen, L.; Li, R.; Zhou, Y.; Zhou, Q. Origin and evolution of deep lithium-rich brines in the southwest Jianghan Basin, central China: Evidence from hydrochemistry and stable isotopes. *J. Hydrol.* **2023**, *626*, 130163. [CrossRef]
38. Li, Z.; He, M.-Y.; Li, B.; Wen, X.; Zhou, J.; Cheng, Y.; Zhang, N.; Deng, L. Multi-isotopic composition (Li and B isotopes) and hydrochemistry characterization of the Lakko Co Li-rich salt lake in Tibet, China: Origin and hydrological processes. *J. Hydrol.* **2024**, *630*, 130714. [CrossRef]

Disclaimer/Publisher's Note: The statements, opinions and data contained in all publications are solely those of the individual author(s) and contributor(s) and not of MDPI and/or the editor(s). MDPI and/or the editor(s) disclaim responsibility for any injury to people or property resulting from any ideas, methods, instructions or products referred to in the content.